香港氣象學會

HONG KONG METEOROLOGICAL SOCIETY

Bulletin

VOLUME 21, 2011

CONTENTS

Editorial 2

The PM2.5 to PM10 Ratio as a Possible Indicator for Identifying Atmospheric Sand-Dust in Hong Kong – an Exploratory Analysis
S.Y. Lau and B.L. Choy 3-20

Influence of the Immediate Environments on Daytime Temperature Variations at Two Urban Stations in Hong Kong
M.C. Wu, Y.Y. Cheng and Y.H. Lau 21-34

A Preliminary Study of the Characteristics of Ultraviolet A (UVA) Radiation in Hong Kong
W.H. Leung, H.K. Yeung, W.M. Ma and W.L. Mok 35-45

Society Events
Popular Science Lecture Series 46
The Second Global Meeting of International Forum of Meteorological Societies 47-48

Editorial

The first paper by S.Y. Lau and B.L. Choy of the Hong Kong Observatory is a study on the possible tool for reporting sand-dust weather in Hong Kong.

The second paper by M.C. Wu, Y.Y. Cheng and Y.H. Lau of the Hong Kong Observatory examines the influence of the micro-environment on daytime temperature variation between the headquarters of Hong Kong Observatory and King's Park Meteorological Station.

The third paper by W.H. Leung, H.K. Yeung, W.M. Ma, and W.L. Mok from the Hong Kong Observatory describes a study of UVA measurement at King's Park.

The Hong Kong Meteorological Society co-organized with the Hong Kong Science Museum to give a Popular Science Lecture Series in November 2011. Four professionals were invited to deliver a talk on "Wind, Fire, Water and Electricity" respectively and explain how these basic elements of nature are related to our daily life. Some photos of the talks are included in this issue.

In November 2011, The Hong Kong Meteorological Society participated in the Second Global Meeting of International Forum of Meteorological Societies held in Xiamen, China. A brief description of this meeting is also included in this issue.

About the cover

The cover is a photograph showing a brilliant sun taken in Tai O by Mr. C.H. Yung.

The $PM_{2.5}$ to PM_{10} Ratio as a Possible Indicator for Identifying Atmospheric Sand-Dust in Hong Kong – an Exploratory Analysis

Lau S.Y. and Choy B.L.
Hong Kong Observatory

Abstract

Sand and/or dust in the atmosphere often lead to a reduction in visibility, and the World Meteorological Organization has stipulated that sand/dust should be suitably stated in weather observation reports. Using the data obtained in a major sand-dust storm event in Hong Kong on 21 March 2010, this paper presents a preliminary study on the possibility of using the ratio of $PM_{2.5}$ to PM_{10} to facilitate weather observers to report sand-dust weather in an operational environment. Tentative results suggested that for Hong Kong, this ratio could serve as a possible tool for discriminating sand/dust originating from East-Asian sand/dust storms from other low visibility phenomena.

1. Introduction

Sandstorms in East Asia originate mostly from Gobi of Mongolia, Northwest China and the other major deserts in Northern China (Figure 1). They occur mainly in late winter and spring, typically from February to April, and are usually caused by strong turbulent winds associated with intense outbreaks of cold air blowing over loose dry soil with no covering vegetation after snow melts. The particle size of sand and dust of these East-Asian sand/duststorms may vary between 0.01 and 100μm (Shao and Dong, 2006). The sand and dust could be carried by the prevailing northeast monsoon to Taiwan, Korea peninsula (Chung and Yoon, 1996), Japan (Zhou et al., 1996), the North Pacific (Husar et al., 2001) as far as Hong Kong (Fang et al., 1999; Lee and Hills, 2003) and possibly beyond.

Because of the large distances from the origins of these East-Asia sand/dust storms, it is rather rare for significant sand/duststorms to affect Hong Kong. Due to their very low concentrations, chemical speciation methods such as X-ray spectrometry have to be employed to ascertain that the sand/dust found in the air samples has their origin in the sand/dust storms. Fang et al. (1999) had found that the concentration of Al (aluminum), Fe (iron) and Ca (calcium) in the dust samples during a dust episode (9-10 May 1996) was much higher than the non-episodic samples. Wai and Tanner (2005) further suggested that the mass ratios of Fe/Al and Mn (Magnesium)/Al could act as good tracers of Asian sand/dust to Hong Kong where sea-salt and other anthropogenic species are normally dominant.

As part of weather services, observations of current weather are made, coded and reported by trained observers, coded and reported. These observations cover, among other things, the state of the atmosphere and any other associated phenomena, such as meteorological meteors, lightning and squalls. Meteorological meteors include lithometeors or dry particulates in the air that impair visibility such as haze, dust, smoke, drifting and blowing sand-dust, sand/duststorms, dust devil and sand whirls. The corresponding classification of these lithometeors in the World Meteorological Organization (WMO) Manual on Codes (WMO No.306) is given in Appendix 1. According to WMO (WMO No.407), haze (WMO Weather Code 05) is defined as suspension in the air of extremely small, dry particles invisible

to the naked eye and sufficiently numerous to give the air an opalescent appearance. WMO further defines dust haze (WMO Weather Code 06) as suspension in the air of dust of small sand particles, raised from the ground prior to the time of observation by a duststorm or sandstorm.

Traditionally observations of lithometeors are conducted by observing the colour of the sky with naked eyes. Haze (weather code 05) imparts a yellowish or reddish tinge to distant bright objects or lights seen through it, while dark objects appear bluish (中國氣象局 , 2007). Dust haze (weather code 06) imparts a yellowish hue to distant object and the sky appears pale white or light yellow. For an atmosphere with a large amount of sand/dust particulates, the reddish hue would be easier to recognize (see Figure 2(a) taken by the author in Beijing on 20 March 2010) thus allowing observers to report the present weather as dust haze (WMO Weather Code 06) rather than more generic haze (WMO Weather Code 05).

However, after the process of long-range transport, most of the larger sand/dust particulates have settled out due to gravitational effects. The colour of the sky is much less distinct (see Figure 2(b) by the weather observer at the Hong Kong International Airport on 22 March 2010). Together with the particulates arising from the local and regional anthropogenic activities, discrimination of haze and dust haze cannot be as readily made. Although concentrations of crustal constituents (Al, Fe, Mn) are good tracers of sand-dust, such concentrations cannot be made available in real-time to weather observers who have to prepare an observation report within 10 minutes.

On 21 and 22 March 2010, the concentrations of particulates reached unprecedented levels in an abrupt manner in Hong Kong. Details are given in Section 3 below. The high particulate concentrations observed at that time in Hong Kong had their origins in the outbreak of an intense sand/dust storm in the Gobi desert. This was later confirmed by the characterization of the soil composition in the Pearl River Delta (PRD) which showed that the concentration of Ca had increased significantly between 21 and 23 March 2010, particularly on 23 March 2010 (廣東省氣象局 , 2011).

However, in cases where the increases in particulate concentrations are less dramatic, it might be even more difficult to immediately associate the increase with sand/dust originating from distant East-Asian sand/dust storms then occurring or had just occurred. The problems associated with the reporting of dust events due to the subjective nature was noted by Shao and Dong (2006). Some kind of supporting tools would come in useful for the observers to report dust haze properly.

In South Korea, the ratio "$PM_{2.5}$ to PM_{10}" with no accompanying rise in $PM_{1.0}$ concentration is used as an indicator to support the weather observer in determining whether the lithometeor is likely to be sand/dust (private communication). Prompted by this, the present study uses $PM_{2.5}$ and PM_{10} data collected locally on 21 and 22 March 2010 to examine the likely applicability of the ratio "$PM_{2.5}$ to PM_{10}" in identifying the presence in Hong Kong's atmosphere of sand/dust originating from East-Asian sandstorms.

The paper is organized as follows. The instruments to collect real-time $PM_{2.5}$ and PM_{10} data are briefly described in Section 2. The sand/dust episode in Hong Kong occurring on 21-22 March 2010 is presented in Section 3. The possibility of using the $PM_{2.5}$ to PM_{10} ratio is discussed in Section 4, and the conclusions are given in Section 5.

2. PM_{10} and $PM_{2.5}$ Data

In this study, the hourly PM_{10} and $PM_{2.5}$ mass concentration data in Hong Kong are obtained from the network of Air Quality Monitoring Stations (AQMS) network operated by Hong Kong's Environmental protection Department (EPD). This network, established some twenty years ago, currently has 14 stations. 11 of these are regional stations and 3 are roadside stations. Figure 3 shows the location of the existing AQMS stations in Hong Kong. All of the AQMSs measure PM_{10} but only 5 of them (Tap Mun, Tung Chung, Yuen Long, Tsuen Wan and Central) also measures $PM_{2.5}$.

PM_{10} and $PM_{2.5}$ mass concentrations are collected by the Tapered Element Oscillating Microbalance (TEOM, Rupprecht & Patashnick Co., Inc., Albany, NY, USA) Series 1400a-PM_{10} and 1400a–$PM_{2.5}$ monitors respectively. They both are true "gravimetric" instruments and are filter-based with the inlet designed to allow only particulate matter of 10μm to remain suspended in the sample air steam. The 1400a-PM_{10} and 1400a–$PM_{2.5}$ monitors differ only in the inlet head.

3. Sand/Dust Episode in Hong Kong on 21-22 March 2010

3.1 Surface-based $PM_{2.5}$ and PM_{10} concentrations

On 19 and 20 March 2010, China experienced one of the most severe sandstorms in recent years. The sand/dust, brought along by the northeast monsoon, caused the PM10 concentration at Tap Mun to rise abruptly soon after the easterly winds at Waglan Island picked up at 07 UTC (Hong Kong Time = UTC + 8 hours) on 21 March 2010. Meanwhile the visibility at Waglan Island fell from 8 km at 06 UTC to around 2 km at 09 UTC.

The rise in PM10 at Tap Mun occurred around 10 hours after that of Kinmen in Taiwan (extracted from the Taiwan Air Quality Monitoring Network http://taqm.epa.gov.tw/taqm/en/HourlyData.aspx) and was followed closely by the sharp rise in PM10 values at Eastern, Causeway Bay and Central stations (Figure 4). About an hour after the rise at Tap Mun, the PM10 at Bao'an (in Shenzhen) also rose rapidly. This was followed by Taipa in Macau about 2 hours later.

The PM10 at Tap Mun continued to increase in the following hours to a record breaking 710μg/m3. This is more than 17 times the annual average (41μg/m3 in 2010) PM10 concentration. The PM10 stayed in the region of 600 μg/m3 during the daytime on 22 March 2010 while the visibility in Hong Kong generally lingered between 2 and 3 km. The visibility in Hong Kong did not improve until late that night.

3.2. Satellite observations

Given the intensity of the March 2010 sand/dust storm in the Gobi Desert, it is interesting to see what some readily available satellite products show vis-à-vis surface observations. The three products presented here are the Moderate Resolution Imaging Spectroradiometer (MODIS) true colour, the split-channel product using MTSAT and the MODIS-Aqua aerosol Deep Blue retrieval.

a) MODIS true colour imageries

The true color satellite imageries from the Earth Observing Satellite MODIS for 20 – 22 March 2010 are given in Figure 5. The locations of sandstorms, portrayed by loose brownish/greyish colors, on 20 and 21 March 2010, agree very well with surface reports (Figure 6). However, on 22 March 2010 an increase in cloudiness over South China made it difficult to discern the full coverage of sand/dust.

b) Split channel products

Figure 7 shows the split channel MTSAT products for from 19 to 21 March 2010. This product, first adopted from a similar product

for detection of volcanic ash, is widely used for detection of Asian sand/dust (Shao and Dong, 2006; Chung, 1992; Kim et al., 2010). It uses the fact that the absorption of clouds (ice and water) is higher in channel around 12 μm (IR2) than 11 μm (IR1) but vice versa for volcanic ash and sand-dust (non-hydrometeor particles) (Prata, 1989; Prata, 1989). Thus (IR2-IR1) will be positive in areas affected by sand/duststorms and appears in colours of yellow to red. It can be seen from Figure 7(a) that the sandstorm over the Gobi desert area is well portrayed by the split-channel satellite picture on 19 March 2010. However, on 21 March 2010, the main area affected by sand/dust was depicted to be near Shanghai (Figure 7(b)) and was less effective in capturing the southward advancement of sand/dust down Taiwan Strait.

c) MODIS-Aqua aerosol Deep Blue

The composite aerosol optical thickness (AOT) retrieved from MODIS-Aqua, which passes over Hong Kong at around 05 UTC, using the Deep Blue algorithm (Hsu et al., 2006) (generated on-line http://disc.sci.gsfc.nasa.gov/giovanni/overview/index.html), for 21 and 22 March 2010 are given in Figure 8(a) and 8(b). Data was sparse around Hong Kong and was not conclusive but the AOT effectively depicted the drop in sand/dust concentrations over Taiwan Strait on 22 March 2010.

4. Use of $PM_{2.5}$ and PM_{10} to Identify Atmospheric Sand-Dust

As sand-dust particulates are carried by the winds away from their source, they settle progressively and the associated airborne concentration drops. With much lower concentration of sand-dust in the air, the refraction of light was not sufficient to make the sky yellow as those locations upstream when the sand-dust reached Hong Kong. It would be even more difficult to differentiate sand-dust and haze using naked eye after dark. As from the above discussion, satellite pictures may not provide all-weather real-time tracking of the dispersion of sand-dust. Aspects of this difficulty have also been reported by other studies on the application of satellite techniques to monitoring East Asian sand/dust storms (Shao and Dong, 2006; 胡秀清等 , 2007). Thus other tools are required to assist weather observers to operationally ascertain whether the deterioration of visibility was due to sand-dust and to report and code accordingly.

The particulates generated by the local anthropogenic activities are relatively small in size. The 5-year averaged (2005 up to 2009 inclusive) ratio of $PM_{2.5}$ to PM_{10} for Central and Tap Mun for the late winter and spring seasons when sand/duststorms are most active (viz. January to May) are 0.65 and 0.68 respectively. This agrees with the result of an earlier pilot study of the chemically speculated $PM_{2.5}$ and PM_{10} data from 1998-99 at Tsuen Wan which showed that the ratio of $PM_{2.5}$ to PM_{10} is around 0.7 (Desert Research Institute, 2006).

On the other hand, the size of the sand-dust particulates is relatively large. The particle size of sand and dust of Asian sand/duststorms may vary between 0.01 and 100μm. From Figure 9, it can be seen that concurrent with the rise in PM_{10}, the $PM_{2.5}$ also rose rapidly in the evening of 21 March 2010. However, the increase of $PM_{2.5}$ was much lower than that of PM_{10}, resulting in a drop of the $PM_{2.5}$ to PM_{10} ratio from 0.6-0.8 before the arrival of sand-dust to less than 0.3 afterwards. This suggests that the ratio of $PM_{2.5}$ to PM_{10}, used in South Korea to assist the weather observers to identifying sand/duststorms, when used in conjunction with the PM_{10} mass concentration (e.g. increasing beyond 200μg/m^3 to avoid false reporting), can possibly serve as an indicator to discriminate sand-dust from haze.

The applicability of the $PM_{2.5}$ to PM_{10} ratio to other sand-dust cases in Hong Kong is now studied. According to Lee et al. (2010), there were over 70 sand-dust days in Hong Kong between 1996 and 2007. Following current practice of reporting haze and mist at a horizontal visibility of below 5000 m in weather reports, cases with horizontal visibility below 5000 m with no reported precipitation of any kind were selected for the study. To further reduce the scope, only those cases with confirmed East Asian origin[1] were included. In total, 6 days between 1996 and 2010, viz. 29 March 2000, 3 March 2001, 14 April 2001, 16 March 2006 and 30-31 March 2006, are selected under these criteria.

These 6 sand-dust days together with the 21-22 March 2010 case are now contrasted against the non-sand dust high PM_{10} event on 6 December 2007, 15 December 2008 and 22 January 2009. The lowest $PM_{2.5}$ to PM_{10} ratio at Tap Mun and Central on these days together with the corresponding PM_{10} mass concentrations, wind direction and speed at Waglan Island are given in Table 1.

As shown in Table 1, except for 16 March 2006 when the winds were light, the $PM_{2.5}$ to PM_{10} ratio on days when Hong Kong was affected by sand-dust are significantly lower than other high PM_{10} days which generally have $PM_{2.5}$ to PM_{10} ratio above 0.5. Thus it would appear that a $PM_{2.5}$ to PM_{10} ratio of 0.5 could, in conjunction with a high PM_{10} mass concentration, be used to distinguish sand/dust and haze for weather reporting in Hong Kong.

1 Sandstorm (weaker ones such as raised dust are not considered) included in the annual report from China within 5 days for cases since year 2000 and the backward trajectory suggested that the air mass could have passed through regions with sand/duststorms. As the annual sand/duststorm report is only available after 2000, for cases before 2000, only those that appeared in other scientific journals were reviewed.

5. Conclusion

The results of this exploratory study suggest that a rapid rise in PM_{10} together with a drop in $PM_{2.5}$ to PM_{10} ratio to below 0.5 appears useful for distinguishing between sand/dust from East-Asian sand/duststorms and particulates generated by the local anthropogenic activities. It is tentatively adopted as a tool for weather observers to operationally assess whether the sand/dust present in the atmosphere in Hong Kong is related to these sand/duststorms. This tool will be further verified and refined in the future.

Acknowledgements

The authors like to thank the Macau Meteorological and Geophysical Bureau, the Shenzhen Meteorological Bureau and the Hong Kong Environmental Protection Department for the provision of PM_{10} and $PM_{2.5}$ data.

References :

1. Chung, Y.S.: 1992. On the observations of yellow sand in Korea. Atmospheric Environment, 26A, pp. 2743-2749.
2. Chung, Y.S. and M.B. Yoon: 1996. On the occurrence of yellow sand and atmospheric loadings. Atmospheric Environment, 30, pp. 2387-2397.
3. Desert Research Institute: 2006. Twelve Month Particulate Matter Study in Hong Kong.
4. Fang, M., M. Zheng, F. Wang, K.S. Chim and S.C. Kot: 1999. The long-range transport of aerosols from northern China to Hong Kong – a multi-technique study. Atmospheric Environment, 33, pp. 1803-1817.
5. Hsu, N.C., S.C. Tsay, M.D. King, J.R. Herman: 2006: Deep Blue Retrievals of Asian Aerosol Properties During ACE-Asia, Geoscience and Remoting Sensing, 44(11), pp. 3180-3195.
6. Husar, R.B., D.M. Tratt, B.A. Schichtel, S.R. Falke, F.

Volume 21, 2011

Li, D. Jaffe, S. Gasso, T. Gill, N.S. Laulainen, F. Lu, M.C. Reheis, Y. Chun, D. Westphal, B.N. Holben, C. Gueymard, I. McKendry, N. Kuring, G.C. Feldman, C. McClain, R.J. Frouin, J. Merrill, D. DuBois, F. Vignola, T. Murayama, S. Nickovic, W.E. Wilson, K. Sassen, N. Sugimoto and W.C. Malm: 2001. The Asian dust events of April 1998. Journal of Geophysical Research, **106 (D16)**, pp. 18317-18330. http://trs-new.jpl.nasa.gov/dspace/bitstream/2014/15739/1/00-1464.pdf.

7. Kim, N.R., Y.S. Kim, J.H. Lee, J.S. Park: 2010. Detection of Asian Dust using the MTSAT-1R Infrared Channels: April 6-9, 2006. International Symposium on Remote Sensing 2010, International Conference on Space, Aeonautical and Navigational Electronics 2010.

8. Lee, Y.C., M. Wenig and X. Yang: 2010. Transport of Dusts from East Asian and non East Asian Sources to Hong Kong During Dust Storm related Events 1996-2007, Atmospheric Environment, 44, pp. 3728-3738.

9. Lee, Y.C. and P.R. Hills: 2003. Cool season pollution episodes in Hong Kong, 1996-2002. Atmospheric Environment, 37, pp. 2927-2939.

10. Prata, A.J.: 1989. Observations of volcanic ash clouds in the 10-12-micron window using AVHRR/2 Data, Int. J. Remote Sensing, 10, pp. 751-761.

11. Prata, A.J.: 1989. Radiative transfer calculations for volcanic ash clouds, Geophys. Res. Lett., 16, pp. 1298-1296.

12. Shao, Y. and C.H. Dong: 2006. A review on East Asian dust storm climate, modeling and monitoring. Global and Planetary Change, 52, pp. 1-22.

13. Wai, K.M. and P.A. Tanner: 2005. Case Studies of Asian Dust Storm Impacts on a Coastal Site: Implication of a good dust storm tracer. Water, Air, and Soil Pollution, 168, pp. 59-70.

14. World Meteorological Organization. Manual on Codes (No. 306).

15. World Meteorological Organization. Manual on the observation of clouds and other meteors (No. 407).

16. Zhou, M., K. Okada, F. Qian, P.M. Wu, L. Su, B.E. Casareto and T. Shimohara: 1996. Characteristics of dust-storm particles and their long-range transport from China to Japan – case studies in April 1993. Atmospheric Research, 40, pp. 19-31.

17. 中國氣象局：2007. 中華人民共和國氣象行業標準 – 地面氣象觀測規範第四部分：天氣現象觀測 .

18. 胡秀清、盧乃錳、張鵬：2007. 利用靜止氣象衛星紅外通道遙感監測中國沙塵暴，應用氣象學報，**18(3)**, pp. 266-275.

19. 廣東省氣象局：2011. 廣東省大氣成分公報 .

Table 1 *The peak PM_{10} and $PM_{2.5}/PM_{10}$ ratio on the 8 days when Hong Kong was affected by sand-dust, contrasted with the non-sand/dust high PM_{10} events on 6 December 2007, 14 December 2008 and 22 January 2009 (shaded). The corresponding prevailing wind direction and mean daily wind speed at Waglan Island of these cases are also given in the table.*

	Peak PM_{10}		Lowest $PM_{2.5}/PM_{10}$		Waglan wind	
Date	Tap Mun $\mu g/m^3$	Central $\mu g/m^3$	Tap Mun	Central	Prevailing direction	Mean wind Speed (km/h)
29/3/2000	221	275	0.32	0.33	060	16.6
3/3/2001	130	214	0.48	0.50	040	18.4
14/4/2001	102	161	0.51	0.47	030	16.8
16/3/2006	133	356	0.64	0.47	030	7.0
30/3/2006	127	184	0.52	0.47	060	23.5
31/3/2006	120	176	0.49	0.41	060	23.9
21/3/2010	715	664	0.24	0.24	090	14.5
22/3/2010	705	716	0.20	0.19	040	23.0
6/12/2007	172	235	0.71	0.75	030	14.3
15/12/2008	148	162	0.63	0.66	010	23.3
22/1/2009	193	257	0.80	0.65	330	6.0

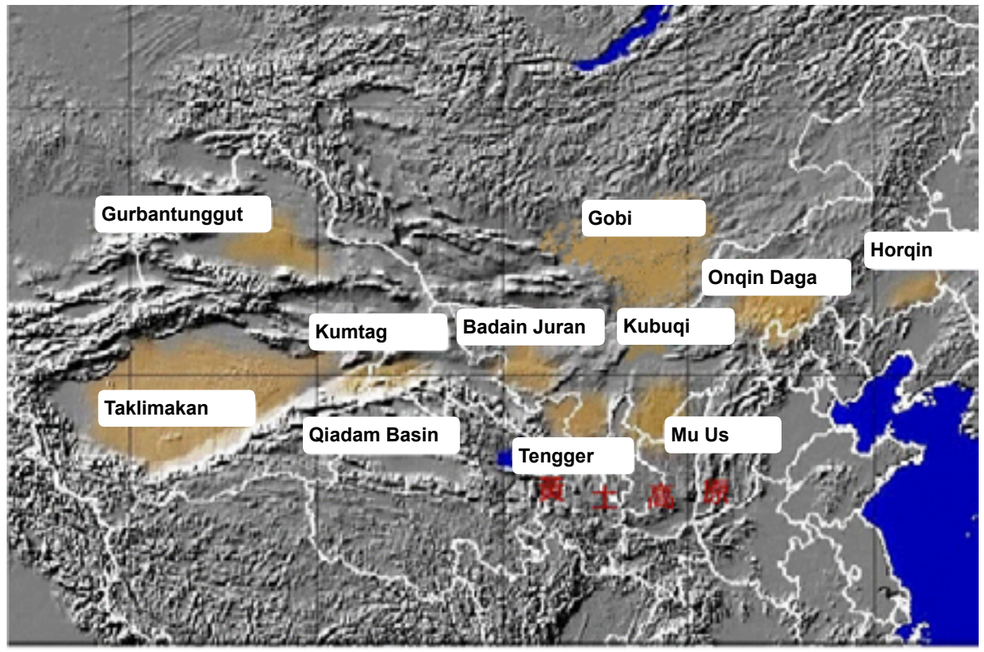

Figure 1. Sources of East Asian sand and duststorms : Taklimakan Desert, Gurbantunggut Desert, Kumtag Desert, Qiadam Basin Desert, Badain Juran Desert, Tengger Desert, Mu Us Desert, Onqin Daga sandy land, Horqin sandy land, Kubuqi, Gobi Deserts and semi-deserts in Mongolia and Loess Plateau.

Figure 2. (a) A picture taken by the author in Beijing on 20 March 2010. No post-processing to the photograph had been made.

Figure 2. (b) A picture taken by the weather observer at the Hong Kong International Airport on 22 March 2010. No post-processing to the photograph had been made.

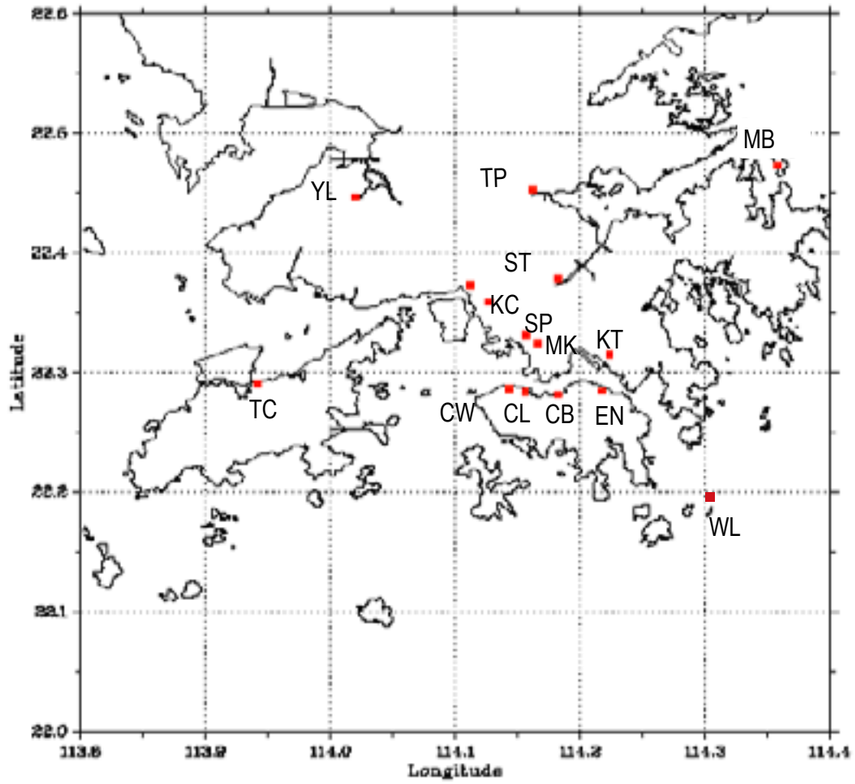

YL – Yuen Long	TP – Tai Po	MB – Tap Mun
TW – Tsuen Wan	ST – Shatin	KC – Kwai Chung
SP – Shamshuipo	MK – Mongkok	KT – Kwun Tong
TC – Tung Chung	CW – Central/Western	CL - Central
CB – Causeway Bay	EN - Eastern	WL – Waglan Island

Figure 3. Location of Air Quality Monitoring Stations (AQMSs) by the Environmental Protection Department in Hong Kong.

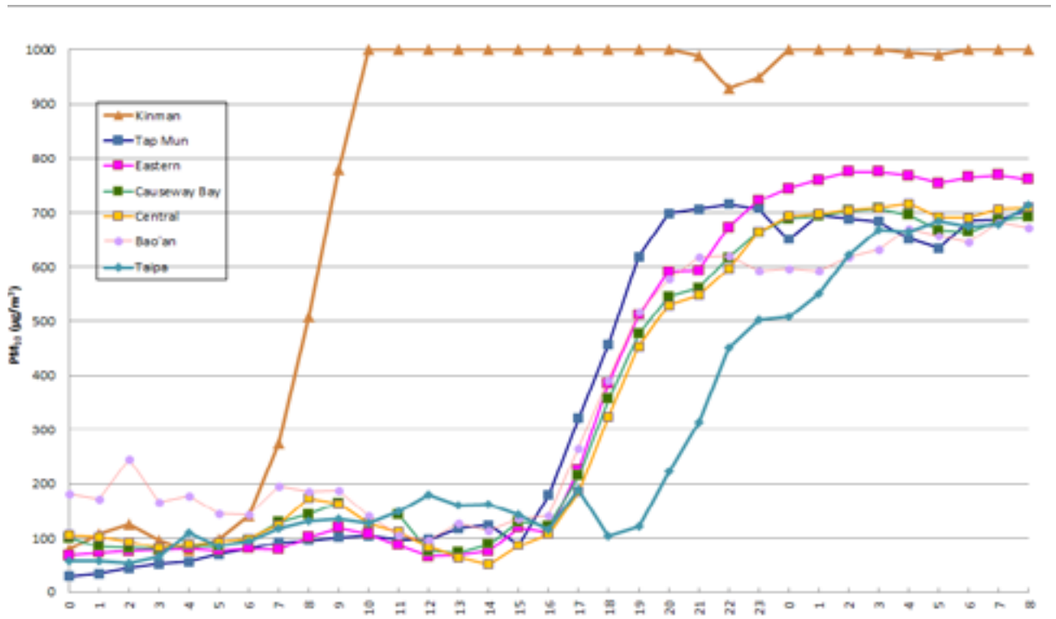

Figure 4. Time series of hourly PM_{10} measurements at Kinmen (Taiwan), Tap Mun, Eastern, Causeway Bay and Central in Hong Kong, Bao'an (Shenzhen) and Taipa (Macau) for 21 – 22 Mar 2010. The PM_{10} values at Kinmen rose above 250μg/m^3 at around 7 a.m., an indication that the sand/dust weather was advancing down Taiwan Strait. 10 hours later, and soon after the easterlies strengthened, the PM_{10} values at Tap Mun also increased sharply, followed closely by that of Eastern. An hour after the rise at Tap Mun, the PM_{10} at Bao'an also rose rapidly to be followed by Taipa in Macau about another 2 hours later.

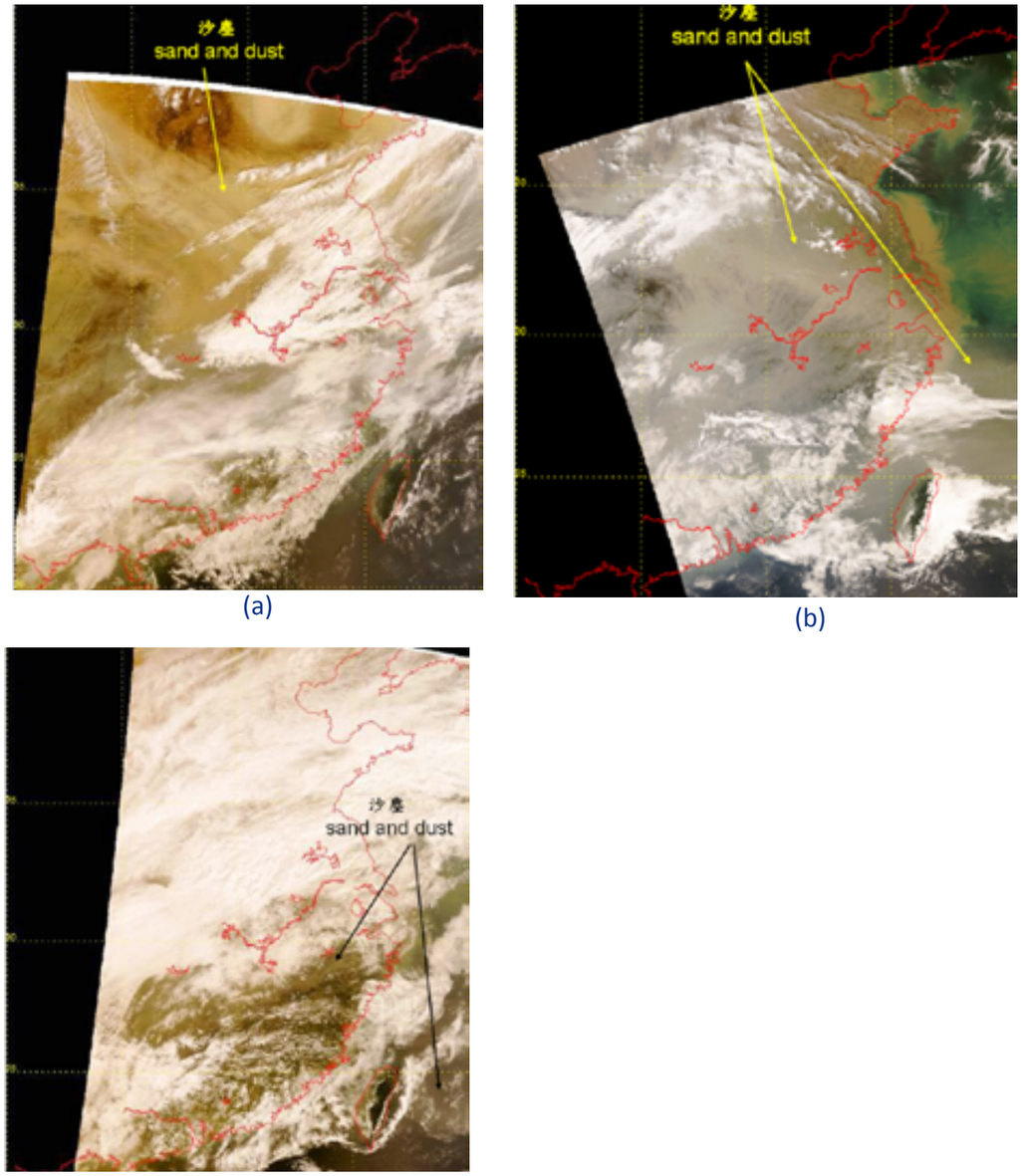

Figure 5. True color image from Earth Observing Satellite (MODIS). (a) 0250UTC 20 March 2010 (Hong Kong Time is 8 hours ahead of UTC time) – sand-dust weather affecting northern China; (b) 0506UTC 21 March 2010 – sand-dust weather affecting Central and Eastern China; (c) 0238UTC 22 March 2010 – sand/dust spread to Taiwan and its adjacent waters. As southern China was generally covered by clouds, sand and dust were not observed from the satellite.

Volume 21, 2011

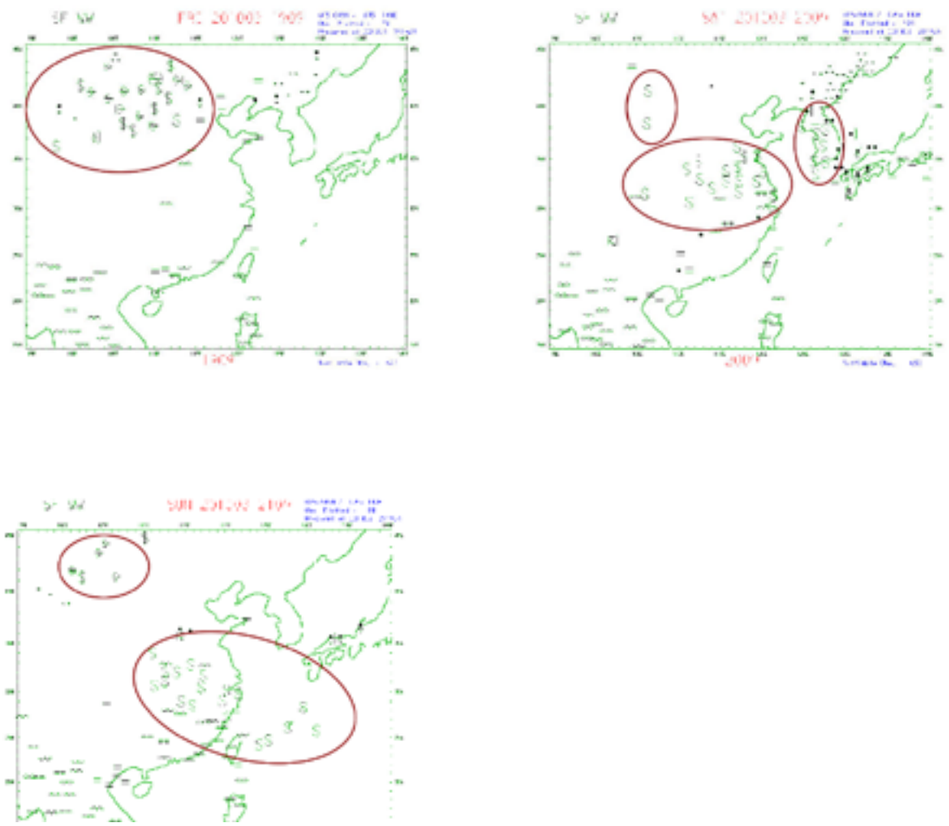

Figure 6 Surface weather reports. Areas affected by sand-dust weather highlighted in brown. (a) 09UTC 19 March 2010 - sandstorm started to develop over Gobi and Tengel deserts; (b) 09UTC 20 March 2010 – sand-dust weather spread further to affect northeast China; (c) 09UTC 21 March 2010 – haze reported along southeast China coast due to the sand-dust weather.

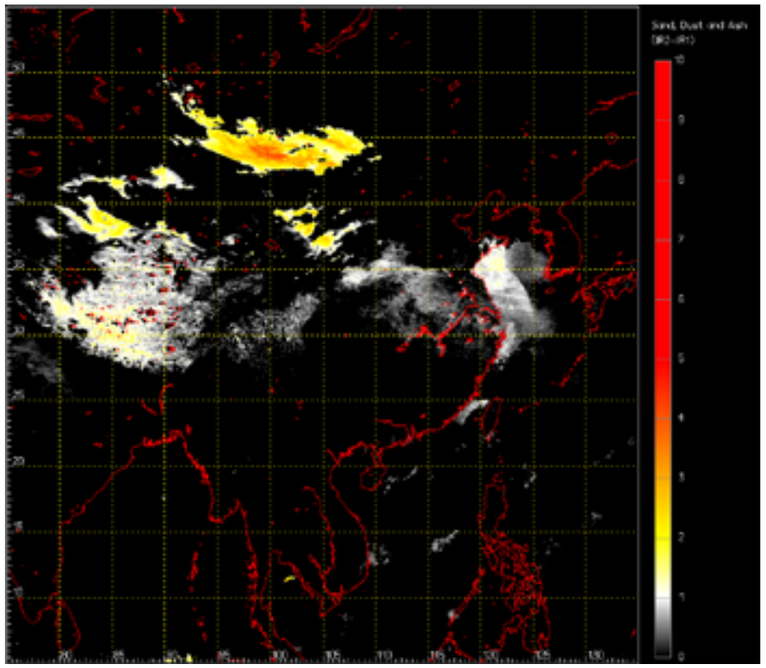

(a) 0330Z 19 Mar 2010

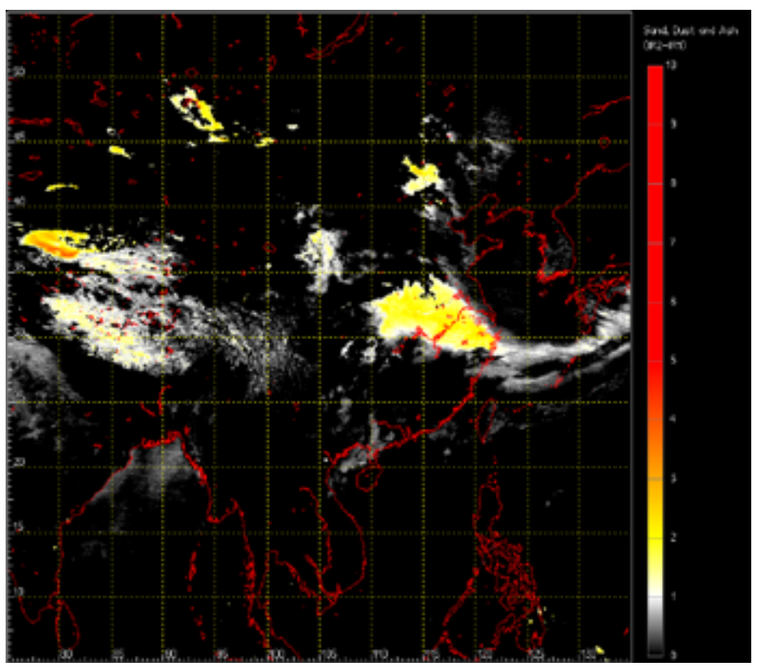

(b) 0330Z 21 Mar 2010

Figure 7. Sand, dust and ash product for 19 and 21 March 2010 based on MTSAT-1R developed by HKO using the "IR split channel" technique.

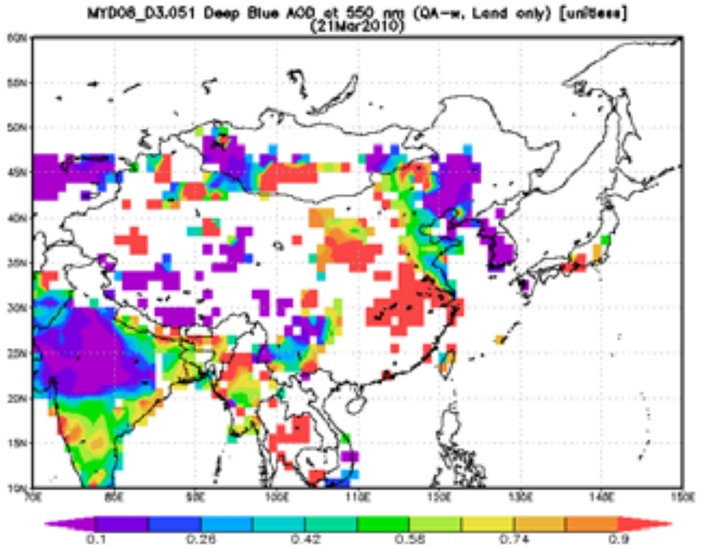

21 Mar 2010

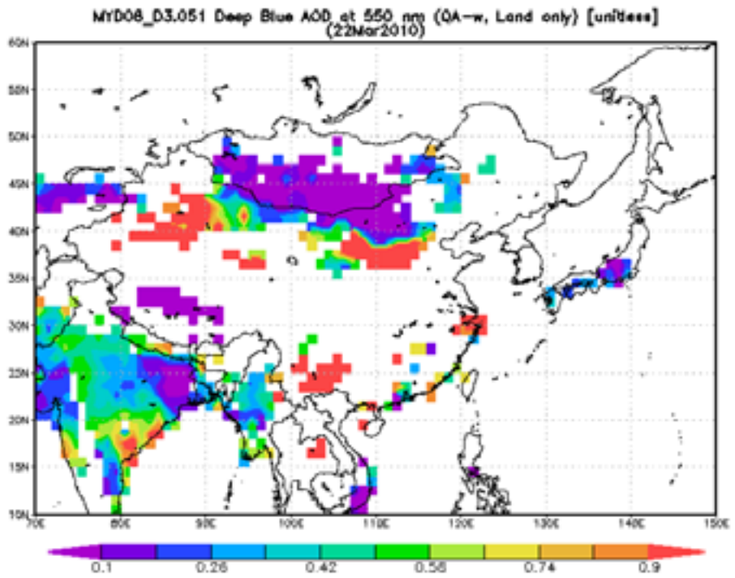

22 Mar 2010

Figure 8 The composite aerosol optical thickness (AOT) retrieved from MODIS-Aqua using the Deep Blue Algorithm for 21 and 22 March 2010

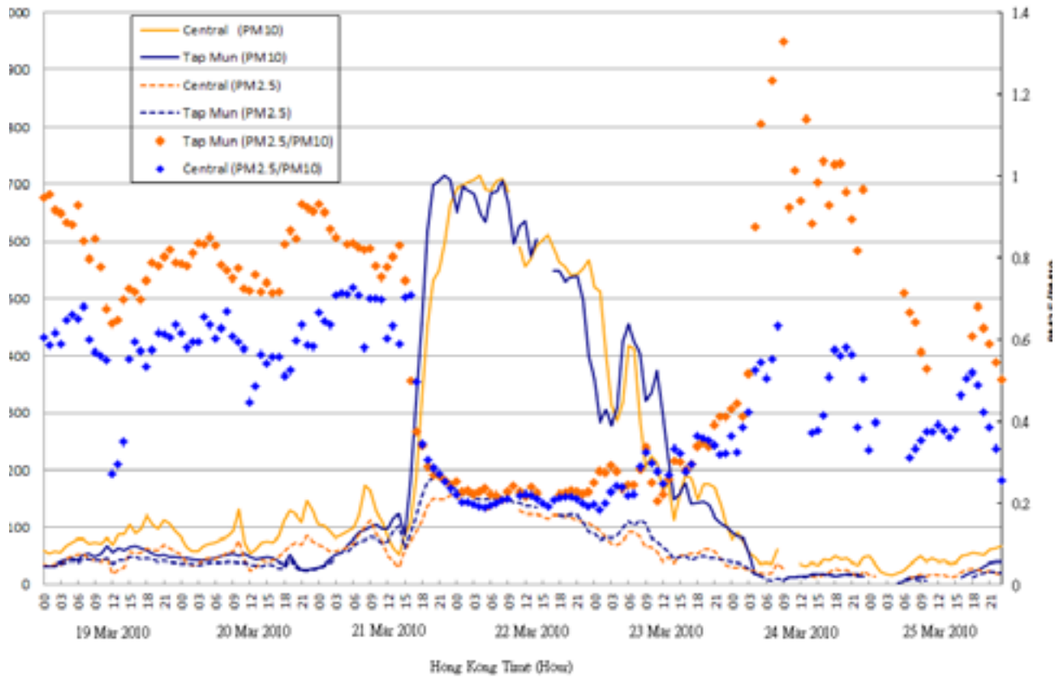

Figure 9. Time series plot of (a) hourly PM_{10} measurements (solid line) at Tap Mun and Central; (b) the hourly $PM_{2.5}$ measurements (dotted line) at Tap Mun and Central; and (c) the ratio of $PM_{2.5}$ to PM_{10} at Tap Mun (dots) and Central for 19 – 23 March 2010. The figure clearly shows that the rise in $PM_{2.5}$ was much lower compared with PM_{10} resulting in a sudden drop in the $PM_{2.5}$ to PM_{10} ratio. The ratio then climbed back to a high value as the concentration of sand/dust in the air gradually dropped.

Volume 21, 2011

CODE TABLES

4677

ww	*Present weather reported from a manned weather station*	
ww = 00–49	No precipitation at the station at the time of observation	
ww = 00–19	No precipitation, fog, ice fog (except for 11 and 12), duststorm, sandstorm, drifting or blowing snow at the station* at the time of observation or, except for 09 and 17, during the preceding hour	
	Code figure	
No meteors except photometeors	00	Cloud development not observed or not observable
	01	Clouds generally dissolving or becoming less developed
	02	State of sky on the whole unchanged
	03	Clouds generally forming or developing
		} Characteristic change of the state of sky during the past hour
Haze, dust, sand or smoke	04	Visibility reduced by smoke, e.g. veldt or forest fires, industrial smoke or volcanic ashes
	05	Haze
	06	Widespread dust in suspension in the air, not raised by wind at or near the station at the time of observation
	07	Dust or sand raised by wind at or near the station at the time of observation, but no well-developed dust whirl(s) or sand whirl(s), and no duststorm or sandstorm seen; or, in the case of ships, blowing spray at the station
	08	Well-developed dust whirl(s) or sand whirl(s) seen at or near the station during the preceding hour or at the time of observation, but no duststorm or sandstorm
	09	Duststorm or sandstorm within sight at the time of observation, or at the station during the preceding hour
	10	Mist
	11	Patches } shallow fog or ice fog at the station, whether on land or sea, not deeper than about 2 metres on land or 10 metres at sea
	12	More or less continuous
	13	Lightning visible, no thunder heard
	14	Precipitation within sight, not reaching the ground or the surface of the sea
	15	Precipitation within sight, reaching the ground or the surface of the sea, but distant, i.e. estimated to be more than 5 km from the station
	16	Precipitation within sight, reaching the ground or the surface of the sea, near to, but not at the station
	17	Thunderstorm, but no precipitation at the time of observation
	18	Squalls } at or within sight of the station during the preceding hour or at the time of observation
	19	Funnel cloud(s)**
ww = 20–29	Precipitation, fog, ice fog or thunderstorm at the station during the preceding hour but not at the time of observation	
	20	Drizzle (not freezing) or snow grains
	21	Rain (not freezing)
	22	Rain (not freezing) } not falling as shower(s)
	23	Rain and snow or ice pellets
	24	Freezing drizzle or freezing rain
	25	Shower(s) of rain
	26	Shower(s) of snow, or of rain and snow
	27	Shower(s) of hail,*** or of rain and hail***
	28	Fog or ice fog
	29	Thunderstorm (with or without precipitation)

A–356 Volume I.1

Appendix 1. Extract from WMO-No. 306 Manual on Codes, Volume I.1

Influence of the Immediate Environments on Daytime Temperature Variations at Two Urban Stations in Hong Kong[1]

M.C. Wu, YY Cheng and YH Lau,
Hong Kong Observatory,
134A Nathan Road, Kowloon,
Hong Kong.

Abstract

The influence of the micro-environment on daytime temperature variation between the headquarters of Hong Kong Observatory (HKO) and King's Park Meteorological Station (KP) is examined. At 1 km from each other, both are urban stations. It is found that on average, the daily maximum temperature at HKO tends to be lower than that at KP in winter when the sun path is lowest. On the other hand, the time of occurrence of daily maximum temperature at HKO tends to lag behind that at KP by an average of about half an hour in summer when the sun path is highest. It is postulated that this daytime temperature variation and such at HKO are influenced by the shielding effect due to the surrounding tall trees and buildings.

1. Introduction

This study explores the influences of the immediate environment on daytime air temperatures at two urban sites in Hong Kong. One is the headquarters of Hong Kong Observatory (HKO) and the other King's Park Meteorological Station (KP). Both are situated in the commercial and residential centre of Kowloon Peninsula (Fig. 1). The horizontal distance between the two stations is about 1 km, and KP's altitude is about 30 m higher than HKO's. Locations of thermometers shed at these stations can be found in SMO 2009.

These two stations are also special for their history. Both stations had once been the reference synoptic station for Hong Kong (SMO 2009). HKO is the oldest meteorological station in Hong Kong with longest data record and the climate condition of Hong Kong is extensively defined by data collected at it (see http://www.hko.gov.hk/cis/climahk_e.htm). KP is the only upper-air station in Hong Kong and it was also designated a climatological station for Hong Kong in 1992 (Wong et al. 1996).

HKO has been taken as a representative urban station (e.g. Wu et al. 2009) in studies related to Urban Heat Island (UHI) effect in Hong Kong. Similarly, KP has also been classified as urban station exhibiting distinct diurnal variations compared to rural surroundings (Mok et al. 2011). In addition, both stations have been shown to under the same urban canopy layer at night in the construction of the urban climatic map (CUHK, 2008).

However, few attempts have so far been conducted to investigate specifically the difference between the temperatures recorded at these stations as a result of the different surrounding environments. That discussions on intra-urban temperature differences are sparse have been noted by Chen et al. (2012).

In reviewing the relationship between air temperature and urban surface geometry, Unger (2009) highlighted the significant influence of the mirco-variations in the immediate environments. Emmanuel (1997) pointed out that the intra-urban temperature variations are influenced by vegetation shade at day but not at night.

[1] Based on a previous paper in Chinese (available online at http://www.weather.gov.hk/publica/reprint/r955.pdf)

Emmanuel and Johansson (2006) showed that the differences are greatest during the daytime. Focusing at Hong Kong's street canyons, using Sky View Factor (SVF) as an indicator of urban geometry, Chen et al. (2012) reported a strong negative relationship between the spatially averaged SVF and daytime intra-urban air temperature differences. The SVF is a measure of the degree to which the sky is obscured by the surrounding for a given point (Grimmond et al. 2001) and a more open environment would have a larger SVF.

Making use of sky view photographs, this study documents the difference in daytime (refers to the duration between sunrise and sunset in the present study) temperature observations made at HKO and KP in summer and winter. In particular, the daily maximum temperature and its time of occurrence are compared. Attempts are then made to relate the differences found to the shielding effects posed by the stations' immediate environments.

Summer is chosen because it has the highest sun path, and winter the lowest. Here, summer refers to the months June to August, and winter December to February.

2. Data and Methodology

2.1 Data

The basic data used in the study are temperature data (include clock hour temperature, daily maximum and minimum temperature) recorded at the HKO Headquarters and KP between 1993[2] and 2009. 1993 is chosen as the starting year as that is the first year in which a full year's data from the KP automatic weather station became available. To eliminate the effect due to rainfall (including trace), only the days with no rainfall record (refer to the condition at HKO for simplicity) are included in the analysis unless otherwise stated. Daily rainfall condition at HKO is available from the website of Hong Kong Observatory at http://www.hko.gov.hk/cis/data/drf_summary_e.htm.

2.2 Aerial and Sky View Photographs

The 1975 aerial photographs used in this study are from the Lands Department Survey and Mapping Office, and the 2007 ones from Google map. The eye-level photographs showing the immediate environments of stations are from the HKO.

The sky view or fish-eye photographs at HKO and KP were taken on-site near the thermometer shed and the screen box respectively, at about 1.2 m above ground level (i.e. at height similar to that of the thermometers). They were taken in December so that tree foliage was minimal. The fish-eye photography is commonly employed to determine the SVF (Grimmond et al. 2001) and for describing urban geometry (Svensson 2004).

[2] Data in December 1992 is also included so that the first winter considered is 1993 which comprises December 1992 to February 1993. The AWS station at KP was established in July 1992.

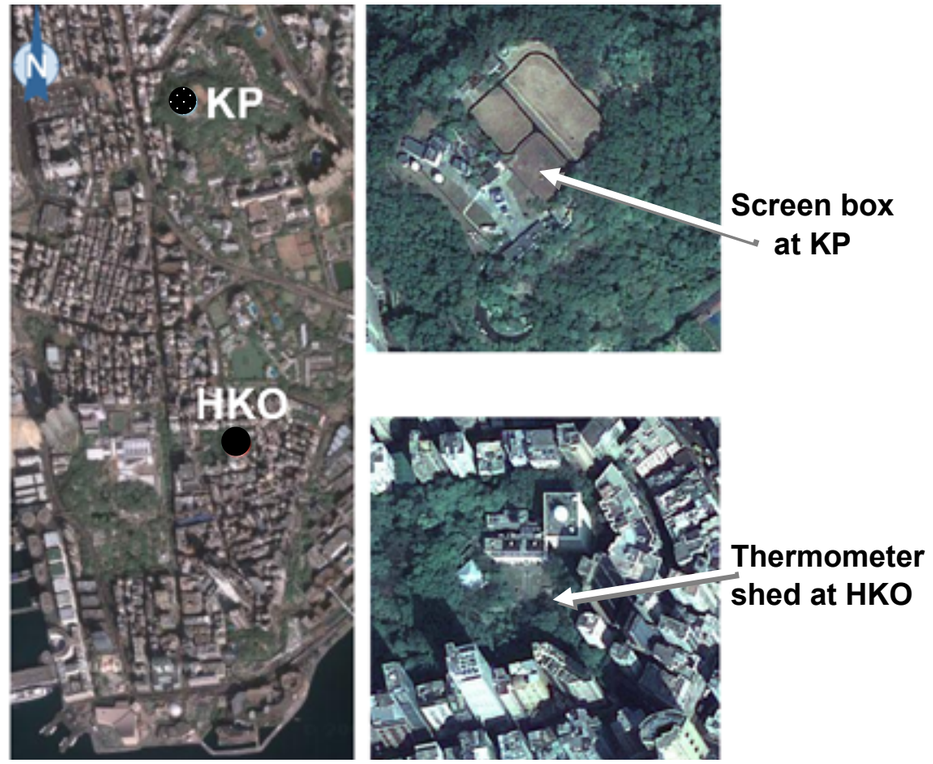

Figure 1 The geographical location of the Hong Kong Observatory Headquarters (HKO) and King's Park (KP). Enlarged photo to the right shows the surrounding environment (covering around 200 km^2) of the thermometer shed and screen box at HKO and KP respectively. Detailed information of these two stations can be found in Hong Kong Observatory (2009).

2.3 Methodology

First of all, the difference in the daily course of temperature between the 2 stations will be presented. With this as background, the rates of change in the hourly temperature (i.e., the hourly temperature minus that of the preceding hour), the daily maximum temperature and its occurrence time at HKO and KP will be compared. The significance of the differences in daily maximum and its occurrence time between HKO and KP will be tested by Student's t-test (Wilks 1999).

The differences yielded by these comparisons will be interpreted in terms of the shielding effects and SVF posed by the corresponding immediate environments as inferred from the sky view photographs (Fig. 2). The authors have ascertained as far as possible that there is no major change in terms of site location, instrumentation or observation practice during the study period at both HKO and KP. Here, the SVF is deduced from sky view photographs by visual inspection. Readers interested in the quantitative estimation of SVF are referred to Unger (2009).

As this study is concerned chiefly with the shielding effects posed by the immediate environments, only daytime temperatures will be considered.

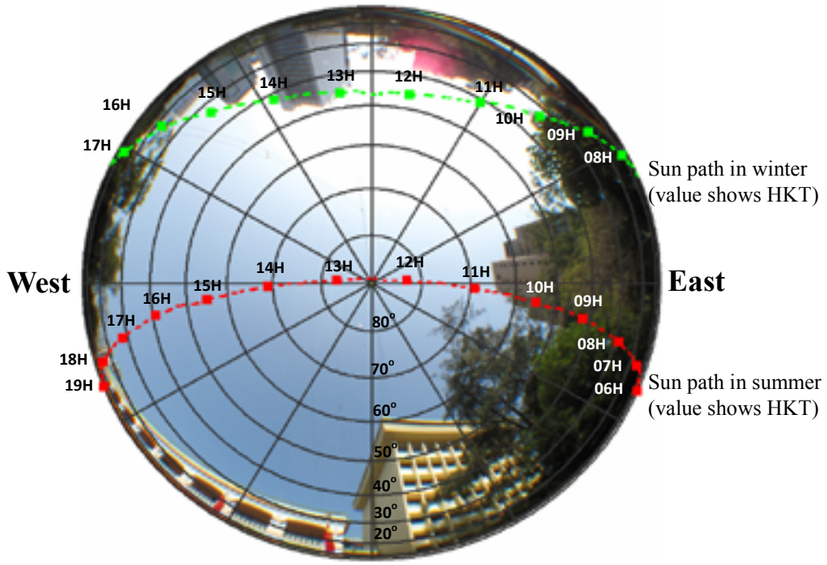

(b) KP

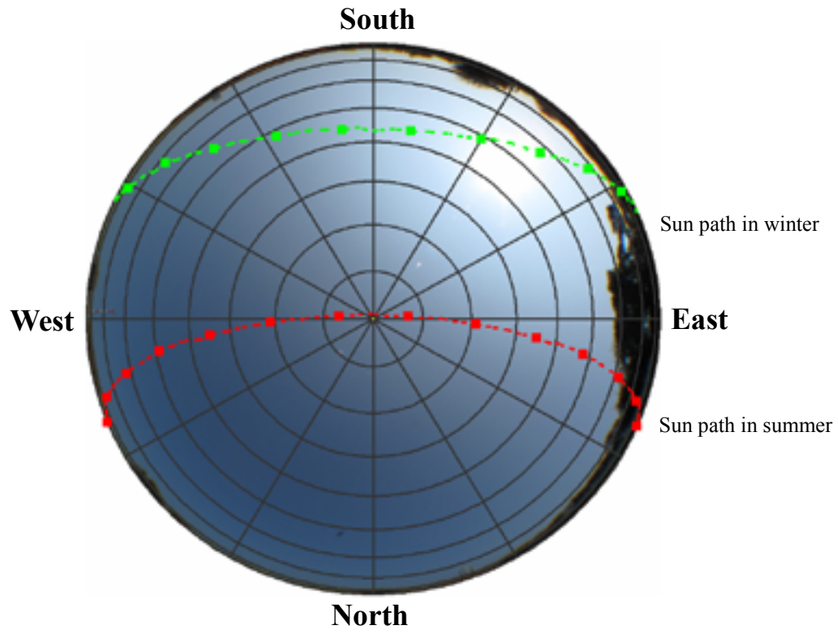

Figure 2. Fish-eye photography taken near (a) the thermometer shed at HKO and (b) the temperature screen box at KP. Both photographs were taken in early December 2010. Sun path in winter (based on the path in mid-January) and summer (based on the path in mid-July) are also indicated.

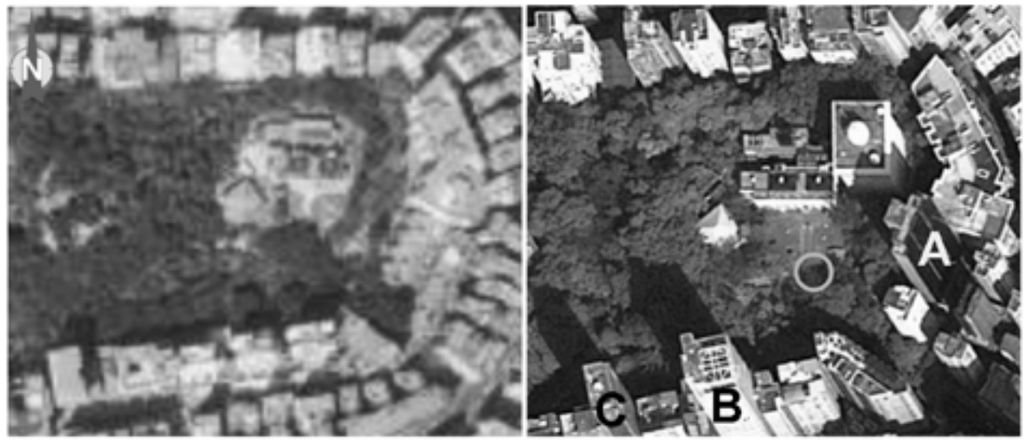

Figure 3. Aerial photographs of the surrounding environment near HKO taken in 1975 (left) and 2007 (right). The labels indicate the buildings that re-developed in late 1990s (Building A was completed in 1997, both B and C in 1999). The grey circle (near the thermometer shed) marks the location of the big banyan tree which fell down in 2006.

Figure 4. Comparison of the immediate environment at HKO in 2005 (left) and 2011 (right). Dashed box highlights the banyan tree in 2005 before it fell down in 2006.

3. Changes in the Immediate Environments

3.1. Hong Kong Observatory Headquarters (HKO)

Figure 3 presents the aerial photographs of the environment near HKO taken in 1975 and 2007. They show the vegetations near the thermometer shed. In September 2006, a big banyan tree located at the southeast of the thermometer shed (or Mat-shed) was blown down by inclement weather (see "The Weather of September 2006" at http://www.weather.gov.hk/wxinfo/pastwx/mws200609.htm).

The influence of the banyan tree in terms of shading effect in daytime and the reduction in SVF can be noted from Figure 4 which compares the environment near HKO in 2005 and 2011.

Moreover, three buildings in the periphery of HKO were re-developed with more storeys in late 1990s (as labeled in Fig. 3). The locations of the banyan tree and the three re-developed buildings as shown in the fish-eye photography are highlighted in Figure 5. Note that the Hong Kong Observatory Centenary building was built in mid-1980s so that it does not appear in 1975 photo.

The fish-eye photographs in Figure 5 shows the changes in the immediate environment at HKO. It can be anticipated that the shielding effect by trees around noon would be more significant in years before the fell down of the banyan tree. Without the building (A in Fig. 5) to the east of HKO in years before 1997, the shielding effect in early morning during summer would be shorten by around an hour. The reduction in the shielding effect by the other two buildings (B and C in Fig. 5) before 1999 is more relevant to winter after noon. It is also noted that the shielding effect in summer may be more apparent than revealed from Figure 2 when vegetation is in full bloom.

It can be anticipated that the SVF at HKO is much larger than that at a typical street canyon in Hong Kong as illustrated in Chen ***et al***. (2012) (their Figure 2). Besides, the SVF at HKO also seems to be larger than at sites situated in public housing estates of Hong Kong as depicted in Giridharan ***et al***. (2007) (their Fig. 1).

Figure 5. Fish-eye photograph at HKO with the 3 re-developed buildings highlighted (see Fig. 3 for the aerial locations). Region of tree foliage of the banyan tree which fell down in 2006 is highlighted as "T".

3.2. King's Park (KP)

Located atop a small hill, KP is less affected by development and re-development of commercial or residential buildings in the vicinity. This is quite obvious from Figure 1. The station's immediate environment has thus been able to remain quite open and unchanged through the years.

Within the station's compound itself, a couple of meteorological instruments have been installed in recent years (Fig. 6, left panel). However, they are located to the western side of the thermometer shed at some distance away and are only vaguely identifiable in the fish-eye photography (Fig. 2). The vegetation in the periphery of the station compound shown in 2004 (Fig. 7) is already present in 1994 (Fig. 6, right panel).

The SVF at KP is obviously larger than at HKO as evident from Fig. 2. Making reference to the fish-eye photography for an urban site (in Germany) that is nearly free of horizontal obstruction as depicted in Blankenstein and Kuttler (2004) (their Fig. 2d), it can be inferred that the SVF at KP is fairly large.

Consistent with a virtually unchanged immediate environment, Alexandersson's (1986) standard normal homogeneity test SNHT shows that none of KP's temperature series under study exhibits inhomogeneity significant at the 5% level.

Figure 6. Eye-level photography of KP in 2011 (left) and 1994 (right, taken from Wong et al 1996) both looking northwestwards.

Figure 7. Vicinity of the screen box at KP (taken in 2004, looking northwards). Trees to the east of the screen box as observed in the fish-eye photograph (Fig. 2) can be seen.

4. Analysis and Results

4.1. Hourly temperature

4.1.1. Winter

Figure 8 shows that during the day, temperatures at HKO are mostly lower than those at KP. The mean duration over which these lower temperatures occur is roughly 8 hours. The greatest daytime temperature difference between HKO and KP is around 14H, and exceeds 1°C.

4.1.2. Summer

In summer, temperatures at HKO are also found to be generally lower than those at KP. Further, the mean duration over which daytime HKO temperatures are found to be lower than KP is about 6-7 hours, about an hour shorter than that noted for winter. The greatest daytime temperature difference between HKO and KP is also smaller, about 0.7oC and peaks earlier, at around 10H.

4.2. Rate of change in hourly temperature

4.2.1. Winter

From sunrise (at around 7H) to around 10H, the temperature rise at HKO, or warming rate, was generally smaller than at KP. This slower rise in morning temperature at HKO, shown in Fig. 9, may be attributable to the sheltering effect of direct sunshine by trees and buildings at HKO to the east as can be seen in Figure 2. As soon as the rate of change at KP attained a maximum at around 10H, temperature at HKO becomes lower than those at KP.

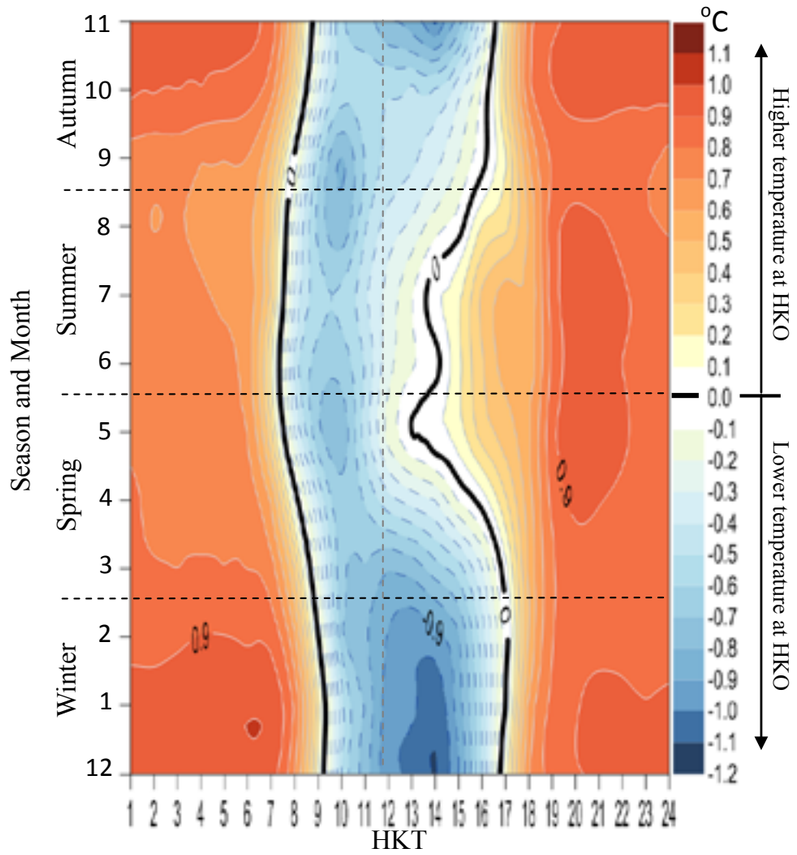

Figure 8 Average temperature difference between HKO and KP (only day with no rainfall record at HKO is included).

From noon onwards, HKO comes under the shade (though intermittently) of the closest trees and buildings as in winter, the sun's elevation angle is still relatively low even at noon and in the early afternoon. Temperatures at HKO stay lower than KP's and the difference with KP reaches a maximum at around 14H, when the temperature at KP starts falling. This also means a lower daily maximum temperature at HKO with respect to KP.

By around 15H, temperatures at both stations begin to fall. Because of its smaller SVF, HKO cools at a slower pace than at KP. By around 17H, HKO's temperatures there become higher than KP. That a smaller SVF will lead to a slower cooling rate has been pointed out in Holmer and Thorsson (2009).

4.2.2. Summer

In early morning, the smaller warming rate at HKO can be said to coincide with the direct sun shielding effect caused by surrounding trees (and tall buildings after 1997). Given the smaller warming rate, temperature at HKO became lower than KP when the warming rate at KP attained a maximum (at around 8H). This is similar to the situation in winter.

Between 11H and 15H, the warming rate at HKO was greater than at KP. This greater warming rate at HKO and the crossing-over in rate of temperature change near noon is distinctively different from winter's case.

The greater warming rate at HKO in summer is likely to be related to the influences of the geometry of surrounding buildings and/or tall trees (as accompanied with reduced SVF). These influences include the inhibition of cooling by convection due to blocking of wind, or multiple reflection of sunlight and faster warming rate of surfaces of nearby buildings (because of lower albedo, see Oke (1982)). How these factors actually operate in conjunction with summer's higher solar altitude and intensity in mid-day is beyond the scope of present study.

From 16H to 19H (i.e. around sunset), the cooling rate at HKO is smaller than at KP. However, compared with winter the difference is small.

4.3. Daily maximum temperature

4.3.1. Winter

Figure 10 shows the time series of the average difference in daily maximum temperature between HKO and KP for winter. As already noted, the daily maximum temperature at HKO in winter is lower than at KP. On average, the difference is 1.2°C, significant at the 5 % level.

4.3.2. Summer

In summer, the daily maximum at HKO is higher than at KP for most years but lower in 2001, 2002 and 2004 (see Fig. 10). The higher daily maximum at HKO in summer can be seen from the higher warming rate in the period between 11H and 15H mentioned earlier. On average, the daily maximum temperature at HKO is higher than KP's by about 0.2°C albeit this figure is not significant at 5 % level. This is in marked contrast with winter's case.

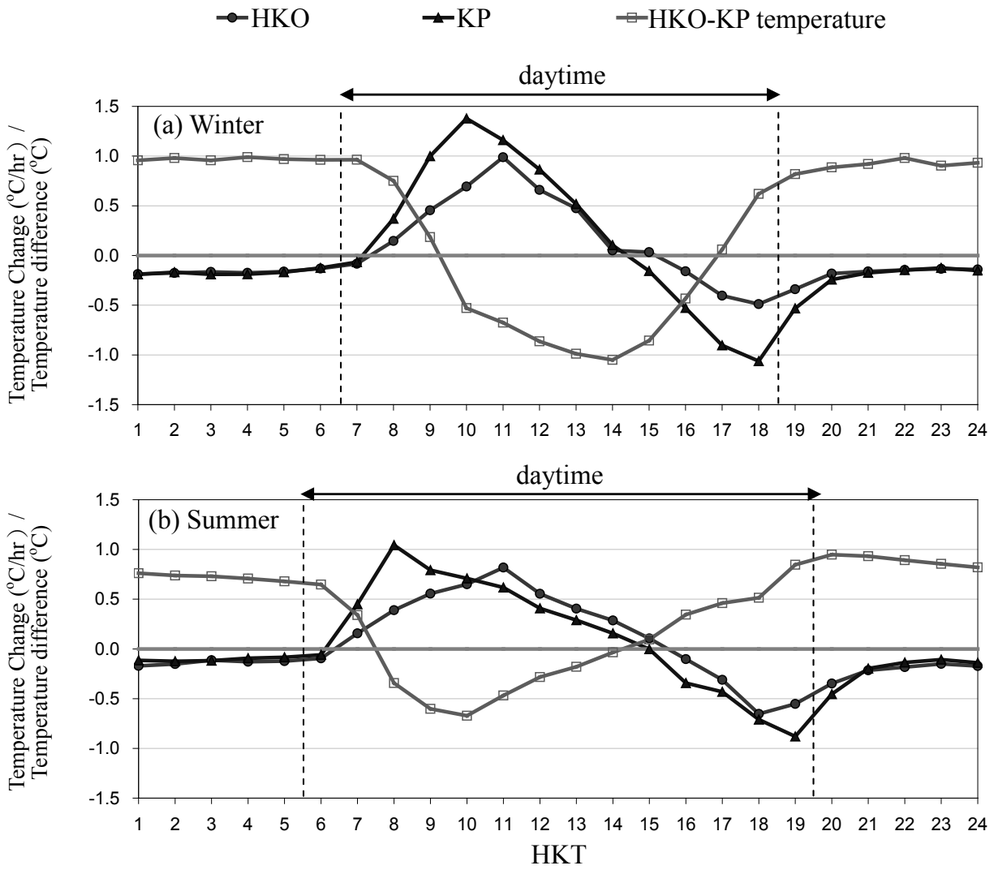

Figure 9. Rate of change in hourly temperature at HKO and KP for (a) winter and (b) summer. Positive (negative) rate indicates temperature is rising (falling). Daytime refers to the period between sunrise and sunset. For completeness, night-time condition is also included. The difference in hourly temperature is also included for reference.

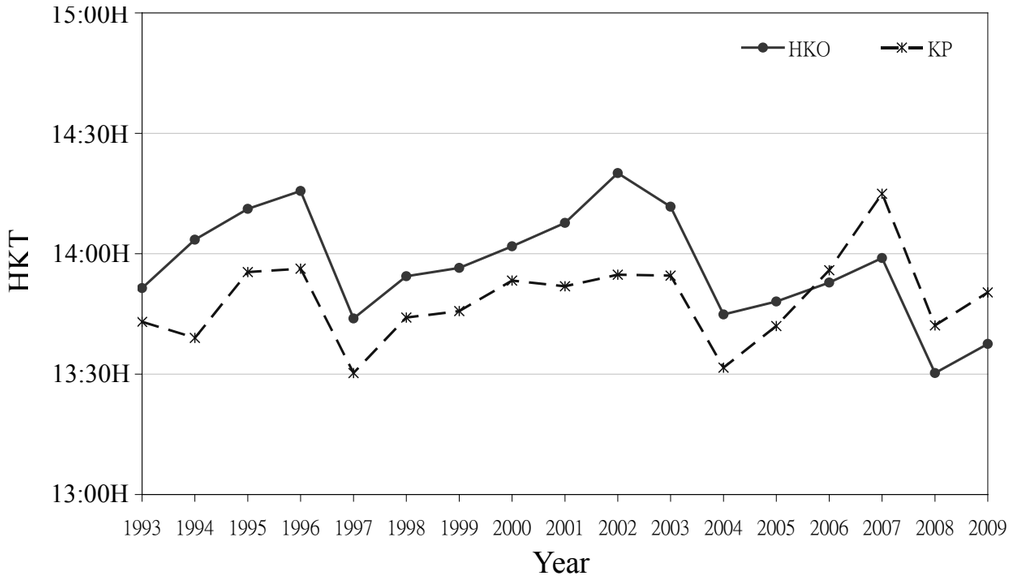

Figure 10. Difference in daily maximum temperature between HKO and KP for summer and winter. Positive (negative) means the daily maximum temperature at HKO is higher (lower) than at KP.

4.4 Time of occurrence of daily maximum

To avoid cases involving cold fronts and cold surges during day-time, situations with daily maximum occurring before noon or after 17H have been excluded in the analysis below.

4.4.1. Winter

The average occurring time of daily maximum is 14:00H[3] at HKO and a bit earlier at around 13:50H at KP. This average of time lag between HKO and KP by less than 10 minutes is marginally not significant at 5 % level.

Figure 11 compares the average occurring time of the daily maximum at HKO and KP for different winters. Evidently, the daily maximum at HKO occurs at a later (earlier) time than at KP in years before (after) 2006 (i.e. 2005/06 winter). The changeover is quite obvious by 2007. Preliminary result shows an apparent increase in the rate of warming near noon at HKO for years after 2006 but not at KP (not shown). Whether this is related to the felling of the banyan tree at HKO is unclear.

[3] All rounded to nearest 5-minute interval.

4.4.2. Summer

In summer, daily maximum at HKO tends to occur at a later time than at KP (Fig. 12). The average occurring time is 14:45H at HKO and 14:15H at KP. In other words, the occurrence time of daily maximum at HKO lagged behind that at KP by roughly half an hour. This difference is significant at the 5 % level.

The apparent delay in the occurrence of daily maximum in summer at HKO may be related to the heat storage hysteresis of building fabric (e.g., McPherson, 1994; Grimmond and Oke, 1999) of the immediate environment at HKO when insolation in summer is stronger and longer.

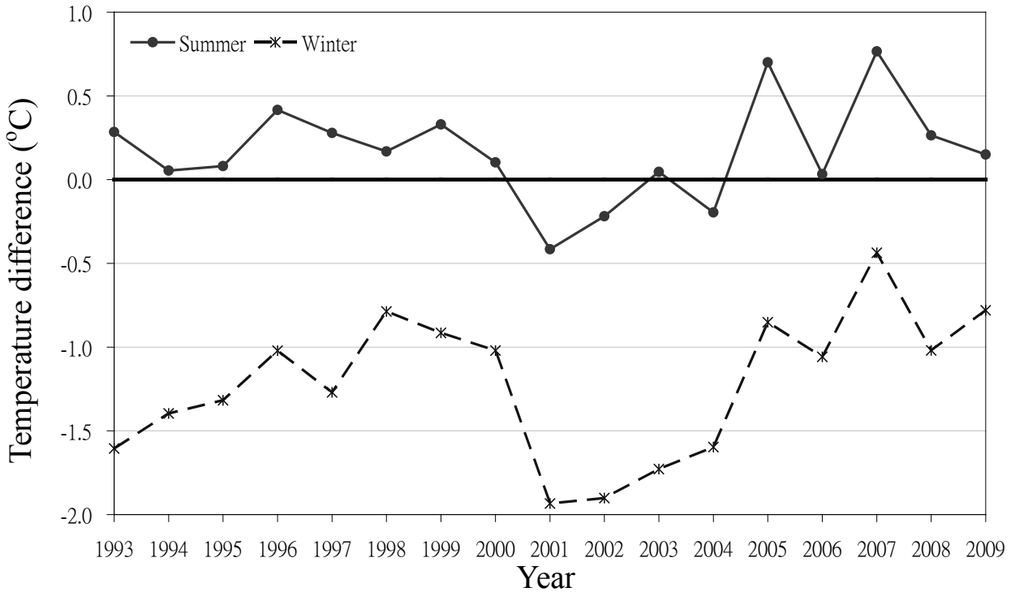

Figure 11. Average occurring time of daily maximum at HKO and KP for winter.

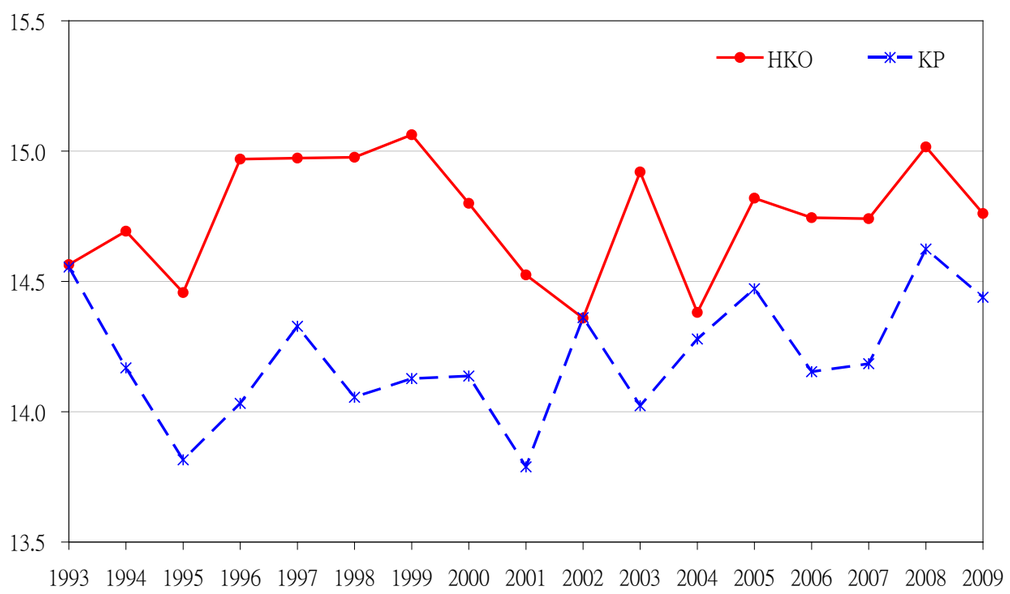

Figure 12. Average occurring time of daily maximum at HKO and KP for summer.

4.5. Summary

The results found in above are summarized in Table 1.

Table 1. Summary of in daytime temperature variations between HKO and KP for winter and summer.

Parameter	Winter	Summer
Hourly temperature	Lower at HKO by > 1oC, peaks around 14H	Lower at HKO by < 1oC, peaks around 10H
Rate of change in hourly temperature	Smaller warming rate at HKO in morning	Smaller warming rate at HKO in the morning but crossover near noon with greater warming rate at HKO
Daily maximum temperature	Lower at HKO by > 1oC	No significant difference
Time of occurrence of daily maximum	HKO slightly lags behind (leads) KP before (after) 2005/06.	HKO lags behind KP by half an hour on average

That HKO's winter daily maximum is lower than KP's by more than 1°C and occurs later than KP's are clear signatures of the influence of the shielding effects and the resulting reduction in SVF at HKO.

5. Conclusion

This study documents the daytime temperature difference between Hong Kong Observatory Headquarters (HKO) and King's Park (KP) in winter and summer.

In both winter and summer, morning temperatures at HKO are lower than those at KP. Also, as a result of the smaller sky view factor, HKO's temperatures rose more slowly than KP's.

In winter, the daily maximum at HKO is significantly lower than KP's by more than 1°C. While summer sees no statistically significant difference in the daily maximum temperatures at HKO and KP, due possibly to the heat storage hysteresis of building fabric of the immediate environment at HKO when insolation in summer is stronger and longer, the time of occurrence of daily maximum temperature at HKO tends to lag behind that at KP by half an hour on average.

The intra-urban variation documented here and its relationship with the skyview and factors such as energy budgets deserves a more rigorous and quantitative study. Hopefully there would be an opportunity to address these aspects in future.

Acknowledgments

The authors would like to thank Choi-hung Yip and Choi-loi Yu for their assistance in providing eye-level photographs of HKO and KP, and Chek-yin Cheng for his help in extracting raw data.

The Hong Kong Observatory Directorate's forbearance in giving the authors' the opportunity to work on this interesting and challenging subject is acknowledged.

Last but not least, the authors like to thank the Chief Editor Dr. W. L. Chang for his comments which helped improve the paper's focus and clarity.

References

1. Alexandersson, H. (1986) A homogeneity test applied to precipitation data, *J. Climatol.*, **6(6)**, 661–675.

2. Blankenstein, S., and W. Kuttler, (2004) Impact of street geometry on downward longwave radiation and air temperature in an urban environment, *Meteorologische Zeitschrift*, **13(5)**, 373-379.

3. Chen, L. and co-authors (2012) Sky view factor analysis of street canyons and its implications for daytime intra-urban air temperature differentials in high-rise, high-density urban areas of Hong Kong: a GIS-based simulation approach. *Int. J. Climatol.*, **32(1)**, 121–136 (Article first published online in 2010)

4. CUHK (2008) Urban climate map and standards for wind environment – feasibility study: Urban climate draft map. Working paper 1A. (available online at http://www.pland.gov.hk/pland_en/p_study/prog_s/ucmapweb/ucmap_project/content/reports/wp1a.pdf)

5. Emmanuel, Rohinton (1997) Summertime Urban Heat Island Mitigation: Propositions based on an Investigation of Intra-Urban Air Temperature Variations, Architectural Science Review, 40(4), 155-164.

6. Emmanuel, Rohinton and Johansson, Erik (2006) Influence of urban morphology and sea breeze on hot humid microclimate: the case of Colombo, Sri Lanka, Climate Res., 3(30), 189-200.

7. Giridharan, R., S.S.Y. Lau, S. Ganesan, and B. Givoni (2007) Urban design factors influencing heat island intensity in high-rise high-density environments of Hong Kong, Building and Environment, 42, 3669-3684.

8. Grimmond, C.S.B., and T.K. Oke (1999) Heat storage in Urban Areas: Local-scale observations and evaluation of a simple model, J. Appl. Met., 38, 922-940.

9. Grimmond, C.S.B., S.K. Potter, H.N. Zutter, and C. Souch (2001) Rapid methods to estimate Sky-View Factors applied to urban areas, Int. J. Climatol., 21, 903–913.

10. HKO (2009) Summary of Meteorological and Tidal Observations in Hong Kong 2009 (available at http://www.weather.gov.hk/publica/smo/smo2009.pdf

11. Holmer, Björn and Sofia Thorsson (2009) Intra-urban nocturnal cooling – A comparison of high-latitude Göteborg, Sweden and Tropical Ouagadougo, Burkina Faso, The seventh International Conference on Urban Climate, 29 June - 3 July 2009 Yokohama, Japan.

12. McPherson, E.G. (1994) Cooling urban heat islands with sustainable landscapes. The ecological city: preserving and restoring urban biodiversity, Rutherford, H.P., R.A. Rowntree and P.C. Muick (eds.), University of Massachusetts Press (Amherst), 151-171 (available at http://www.fs.fed.us/psw/programs/uesd/uep/products/cufr_82_EM94_59.PDF)

13. Mok, H.Y., M.C Wu, and C.Y Cheng (2011) Spatial Variation of the Characteristics of Urban Heat Island Effect in Hong Kong, J Civil Engineering and Architecture, 5(9), 779-786.

14. Oke, T.R., (1982) The energetic basic of the urban heat island, Quart. J. R. Met. Soc., 108(455), 1-24.

15. Svensson, M K. (2004) Sky view factor analysis – implications for urban air temperature differences. Meteorol. App., 11(3), 201–211.

16. Unger J. (2009) Connection between urban heat island and sky view factor approximated by a software tool on a 3D urban database. Int. J. Environment and Pollution, 36, 59–80.

17. Wilks, D.S. (1999) "Statistical Methods in the Atmospheric Sciences". Academic Press, 467 pp

18. Wong, S.K., K.P. Wong and K.B. Lam (1996) Climatological normals for King's Park Meteorological Station, HKO Tech. Note (Local) No. 67, 25pp.

19. Wu M.C., Y.K. Leung, W.M. Lui, and T.C. Lee (2009) A study on the difference between urban and rural climate in Hong Kong. Meteorology, 35(2), 71-79 (in Chinese with English Abstract).

A Preliminary Study of the Characteristics of Ultraviolet A (UVA) Radiation in Hong Kong

W.H. Leung, H.K. Yeung, W.M. Ma, and W.L. Mok
Hong Kong Observatory

Summary

Ultraviolet A (UVA) radiation is one of the main components of solar radiation. In the past, UVA radiation was often neglected by people since it would not cause immediate sunburn to skins. However, recent studies showed that over-exposure to UVA radiation may also be harmful to our skin.

The Hong Kong Observatory started measurement of UVA radiation at the King's Park Meteorological Station in mid 2009. This paper analyzes the UVA radiation data collected in Hong Kong between 1 August 2009 and 31 July 2010 with a view to gaining some insight into the basic characteristics of UVA radiation in Hong Kong.

In common with findings in studies for other places, results show that intensity of UVA radiation correlate well with the UV index. Also, UVA radiation is less scattered by the atmosphere than UVB radiation. In the morning, evening or in winter when the solar elevation is relatively small, the intensity of UVA radiation would change with a slower rate than that of UVB radiation.

1. Introduction

Ultraviolet (UV) radiation can be classified into ultraviolet A (UVA), ultraviolet B (UVB) and ultraviolet C (UVC) radiations according to their wavelengths. UV radiation reaching the earth's surface consists mostly of UVA and some UVB radiation, as all UVC and most of the UVB radiation is absorbed by the atmosphere. Although much less UVB radiation manages to reach the ground than UVA radiation, it is well-recognized that UVB radiation is much more instrumental in causing sunburn and skin cancer. UVA radiation is known to cause the darkening of skin, aging of skin as well as hastening the occurrence of wrinkles. However, as it does not cause immediate sunburn, discussions on UVA radiation have been in the main overlooked in the past. In recent years, some studies pointed out that absorbing excessive UVA radiation would have potential health impact (Lim and Rigel, 2007).

As recommended and introduced by the World Health Organization (WHO), UV index is the de facto reference to measure the effect of solar UV radiation on human skin. The higher the UV index, the more likely will be the damage to skins. The Hong Kong Observatory has been measuring and disseminating UV index to the public since 1999, and providing UV index forecast service since 2006.

From the calculation of UV index (WHO, 2002), the weighting factors of UVA radiation in the erythemal action spectrum are much less than those of UVB radiation. UVB radiation is therefore the major contributor for the UV index. It would be worthwhile to compare the behaviour of UVA and UVB radiation in Hong Kong.

In line with recent thinking, the

Observatory began making measurements of UVA radiation in August 2009. This paper analyzes the data collected from 1 August 2009 to 31 July 2010 with a view to obtaining a preliminary understanding of the characteristics of UVA radiation in Hong Kong. Studies included documenting quantitatively the diurnal and seasonal variations of UVA radiation, examining its maximum value as compared with other places, comparing its characteristics with those of UVB, and studying the effects of cloud cover.

2. UVA Radiation Measurements

The Observatory measures UVA radiation at the King's Park Meteorological Station (latitude 22°19', longitude 114°10'), which is located in the urban area of Hong Kong at an altitude of 65 metres above sea level. The sensor used is the Kipp & Zonen UVS-A-T model with a spectral response of wavelengths from 315 to 400 nm. It measures the one-minute average of UVA radiation flux, i.e. irradiance, in watt per metre square (W/m^2).

In this study, UVA radiation data recorded from 1 August 2009 to 31 July 2010 were analyzed. Following standard practice, the average radiation flux or irradiance of UVA radiation over a short time interval (e.g. 1 minute, 15 minutes or 1 hour) is measured in watt per square metre (W/m^2), while the accumulated UVA radiation energy over a period (e.g. 1 day or 1 month) is measured in kilojoule per square metre (kJ/m^2). The daily maximum UVA irradiance is defined as the maximum of all the 15-minute mean UVA irradiance values recorded during the day.

3. Some Characteristics of UVA Radiation in Hong Kong

Table 1 shows the ranges and average values of the maximum daily UVA irradiance in different months from August 2009 to July 2010. It can be seen that the highest daily maximum value is 65.0 W/m^2 which occurred in July. This value is comparable to the highest daily maximum of 69 W/m^2 recorded in Taiwan in July 2010 (Environmental Protection Department, Executive Yuan, Taiwan, 2010).

Figure 1 shows the diurnal variation of UVA irradiance averaged during a whole year period and during different seasons. For all seasons, the hourly average UVA irradiance peaks at around 1 p.m., as the solar elevation reaches its maximum in Hong Kong around noon to 1 p.m.. Figure 2 shows the monthly variation of the daily average and the daily maximum values of accumulated UVA radiation energy. The highest values of both the daily average and daily maximum accumulated UVA radiation energy were recorded in July. The daily maximum accumulated UVA radiation energy in summer is almost double that in winter. These seasonal changes are mainly due to UVA radiation being absorbed and scattered by the atmosphere under different solar elevations in different seasons.

4. Comparison with UVB

4.1 Correlation

As UVB radiation is not measured directly, following Mckenzie *et al.* (2004), the UVB irradiance values used in the correlation (and other analysis here) are approximate values derived by multiplying the UV index by a constant.

Figure 3 shows the time series of the daily accumulated UVA and UVB radiation energy from 1 August 2009 to 31 July 2010. The variations of the two series are in step with each other. Figure 4 is a scatter plot of the daily accumulated UVA and UVB radiation energy during the same period. The correlation coefficient (r) is computed to be 0.97. It is significant at the 5% level, indicating very high level of relationship between UVA and UVB. Since our values for UVB radiation are derived from the UV index, it might be inferred that the correlation between UVA radiation and the UV index should also be high.

4.2 Diurnal variation

Figure 5 shows the diurnal variation of the irradiance of UVA and UVB radiation. It is noted that during the same time interval, the change in irradiance of UVA radiation is less than that of UVB radiation. This is because UVA radiation has a longer wavelength (315-400 nm) than that of UVB radiation (280-315 nm) and therefore scattering of UVA radiation by air and water particles will be less prominent. This phenomenon is more pronounced in the morning and during sunset when the sun's elevation angle is small. For example, as shown in Figure 5, the irradiance of UVB radiation was around 7 times of its original value as the sun's elevation angle increased gradually from 8 a.m. to 10 a.m., but the UVA irradiance only increased to over 3 times of its original value during the same period.

Figure 6 shows the diurnal variation of the ratio between the irradiance of UVA and UVB radiation under clear sky condition (with total cloud amount of 0 to 2 oktas). In the morning and during sunset when the sun's elevation angle is small, scattering of UVB radiation is more prominent and therefore the ratio between the irradiance of UVA and UVB radiation would be larger. Around noon, as the sun is almost at its culmination, scattering of UVB radiation is less significant and the ratio between the irradiance of UVA and UVB radiation would be smaller.

4.3 Seasonal Variation

Figure 7 shows the monthly average values of the daily accumulated energy of UVA and UVB radiation from 1 August 2009 to 31 July 2010. The amount of average daily accumulated energy for UVB radiation in summer is around 4 times of that in winter, but the seasonal difference for that of UVA radiation is only about 3 times. Furthermore, during the period between May and August, the accumulated energy for UVB radiation accounts for 49% of the annual amount, while the accumulated energy for UVA radiation only accounts for 44% of the annual amount. Therefore, when compared to UVB radiation, UVA radiation has less seasonal change.

5. Effect of clouds on UVA Radiation

Water droplets in clouds will absorb, reflect and scatter incident UV radiation and therefore reducing the intensity of UVA radiation reaching the ground surface in most cases. Figure 8 shows the plots of daily accumulated UVA radiation energy against daily average total cloud cover in different seasons. It can be seen that, for all seasons, the daily accumulated UVA radiation energy only decreases significantly when the cloud cover exceeds 80%. This is because when the amount of cloud cover is small, part of the UVA radiation could still pass through the narrow gaps between the clouds.

Apart from cloud cover, the intensity of UV radiation is also affected by the cloud type (Bais *et al.*, 1993). For example, high level cirrus clouds would allow a significant portion of UV radiation to pass through, while stratocumulus clouds in the mid atmosphere can absorb a larger amount of UV radiation. Figure 9 shows the variation in UVA irradiance from 26 to 28 March 2010. During the period from 2 p.m. to 7 p.m. on 26 March and from 8 a.m. to 1 p.m. on 28 March, Hong Kong was partly covered by high level cirrus clouds, and it was cloud free for the rest of the periods. During these two days, only very small decreases in the UVA irradiance were observed. In contrast, Hong Kong was covered by stratocumulus clouds of 7 oktas on 27 March 2010, and the irradiance of UVA radiation was reduced significantly.

Occasionally, the irradiance of UVA

Volume 21, 2011

radiation may be enhanced due to reflection at cloud edges (Kimlin *et al.*, 2002). This is demonstrated in the case on 8 July 2010 (not shown). On that day, there were 4 oktas of cumulus clouds and with a visibility of 27 kilimetres at the Hong Kong Observatory. In another case on 5 July 2010, it was generally sunny with only 2 oktas of cumulus clouds and the visibility at the Observatory was 23 kilometres. Although the amount of cloud cover on 8 July was larger, the maximum UVA irradiance reached 58.5 W/m^2 which was higher than that of 55.7 W/m^2 on 5 July.

Furthermore, it also would appear from the instance shown in Figure 10 that there is no significant difference between the effect of clouds on UVA and UVB radiation. Figure 10 shows the ratio of the irradiance of UVA and UVB radiation on sunny days (3, 4 and 5 December 2009, with 2 oktas of clouds or less) and on cloudy days (17, 19 and 26 December 2009, with 7 oktas of clouds).

It is evident that the ratio is quite independent of cloud cover.

6. Discussion and Conclusion

The UVA radiation data collected in Hong Kong between 1 August 2009 and 31 July 2010 was analyzed in this paper. Results indicate that the intensity of UVA radiation and UV index correlate strongly with each other. UVA radiation is less scattered by the atmosphere when compared to UVB radiation. When the solar elevation is small (in the morning, evening or in winter), the irradiance of UVA radiation changes with a slower rate than that of UVB radiation.

As the UVA radiation data analyzed in this paper cover only one year, further studies would need to be carried out when more data are available.

References

1. Bais, B.A., C.S. Zerefos, C. Meleti, I.C. Ziomas and K. Tourpali, 1993: Spectral Measurements of Solar UV-B Radiation and its Relations to Total Ozone, SO_2 and Clouds. J. Geophys. Res., 98, D3, 5199-5204.

2. Environmental Protection Department, Executive Yuan, Taiwan, UVA web page, 2010: http://cats.gcc.ntu.edu.tw/EPA/Welcome.html.

3. Kimlin M.G., A.V. Parisi, J. Sabburg and N.J. Downs, 2002: "Understanding the UVA environment at a sub-tropical site and its consequent impact on human UVA exposure". Photochem. Photobiol. Sci., 1, 478-482 pp.

4. Lim H.W., and Darrell S. Rigel, 2007: "UVA: Grasping a better understanding of this formidable opponent". Skin & Aging, 62 pp.

5. McKenzie R., D. Smale and M. Kotkamp, 2004: "Relationship between UVB and erythemally weighted radiation". Photochem. Photobiol. Sci., 3, 252-256 pp.

6. World Health Organization, 2002: Global Solar UV Index – A Practical Guide.

Month	Average value (W/m^2)	Standard deviation (W/m^2)	Range (W/m^2)
January	29.4	9.8	9.9-44.3
February	22.8	10.8	5.5-45.3
March	28.4	13.0	5.0-50.95
April	31.7	14.6	5.3-55.3
May	43.2	12.7	18.7-59.6
June	43.3	15.6	11.6-60.9
July	54.9	9.4	27.8-65.0
August	46.4	9.8	19.1-57.3
September	44.4	11.4	8.7-57.0
October	40.3	7.3	20.6-53.2
November	35.3	9.0	13.6-47.9
December	27.0	9.7	9.3-39.5

Table 1 Monthly statistics of daily maximum UVA irradiance (Data period: 1 August 2009 to 31 July 2010)

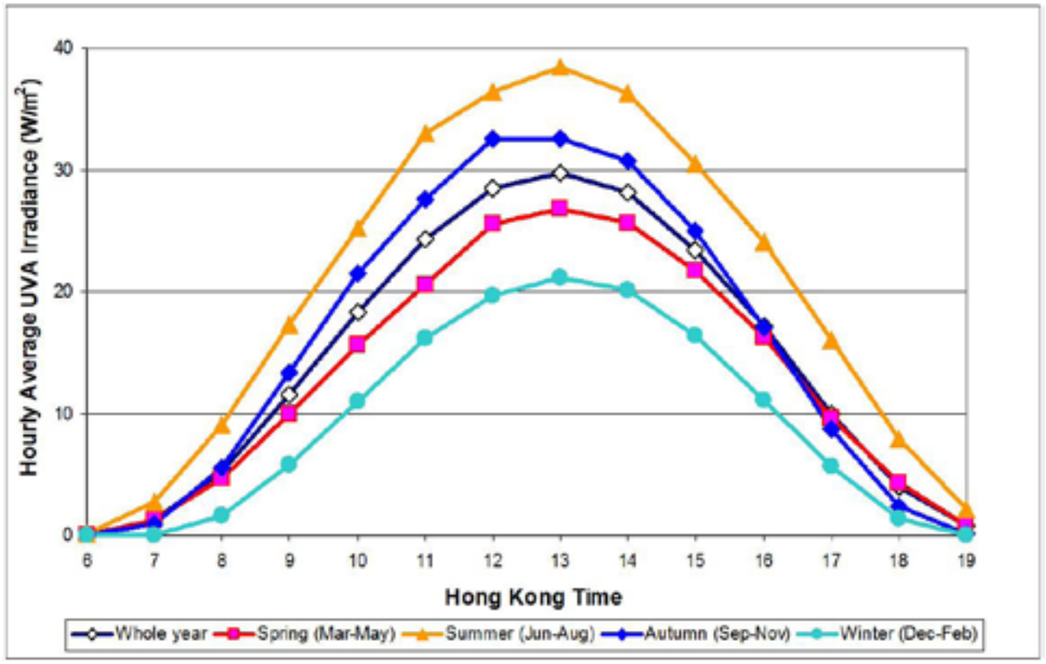

Figure 1. Diurnal variation of UVA irradiance averaged during a whole year period and during different seasons
(Data period: 1 August 2009 to 31 July 2010)

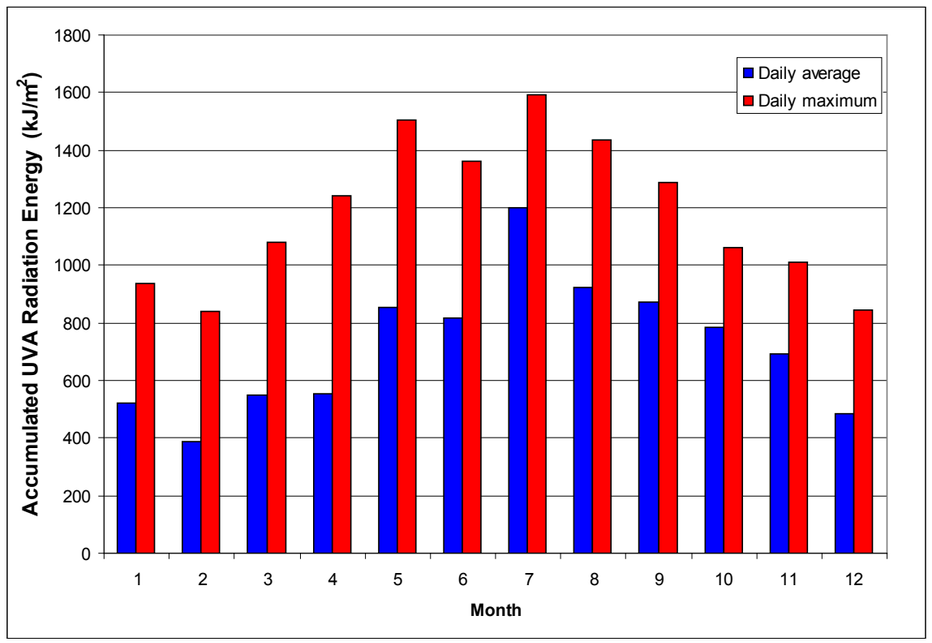

Figure 2. Monthly variation of daily average and daily maximum accumulated UVA radiation energy
(Data period: 1 August 2009 to 31 July 2010)

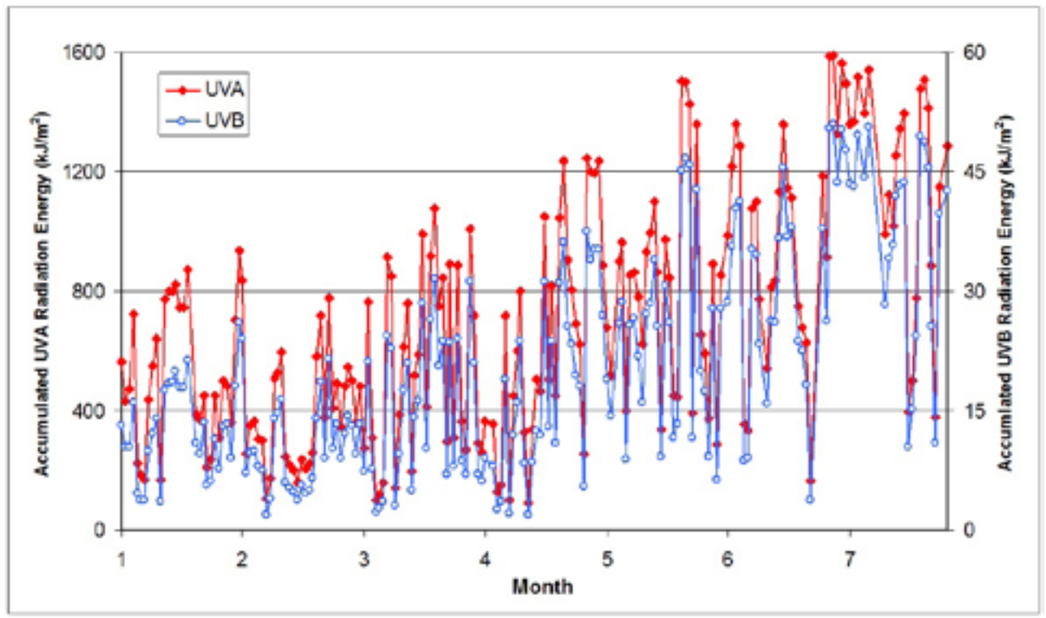

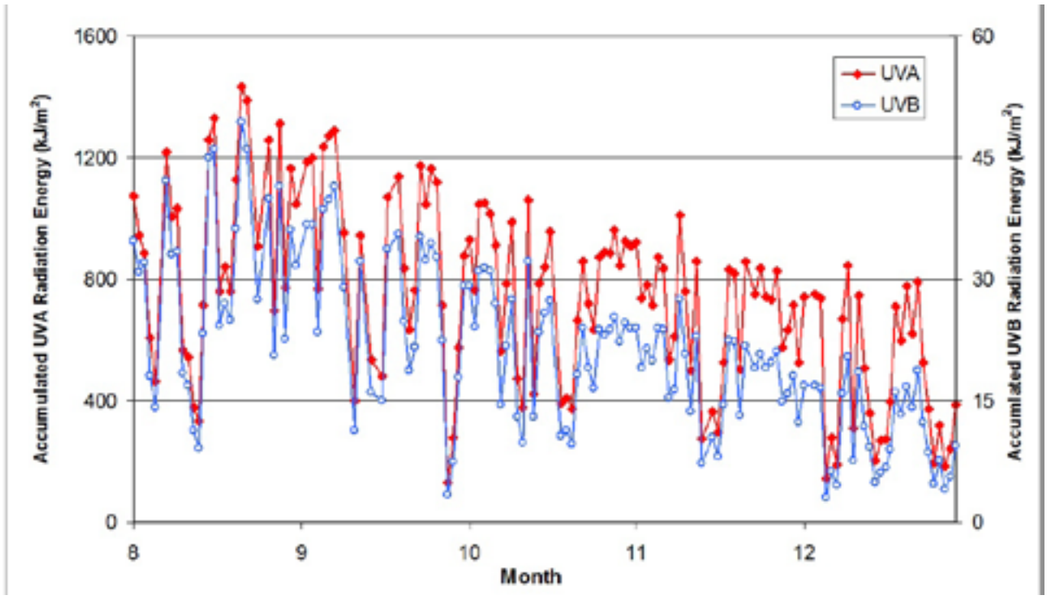

Figure 3. Time series of daily accumulated UVA and UVB radiation energy
(Data period: 1 August 2009 to 31 July 2010)

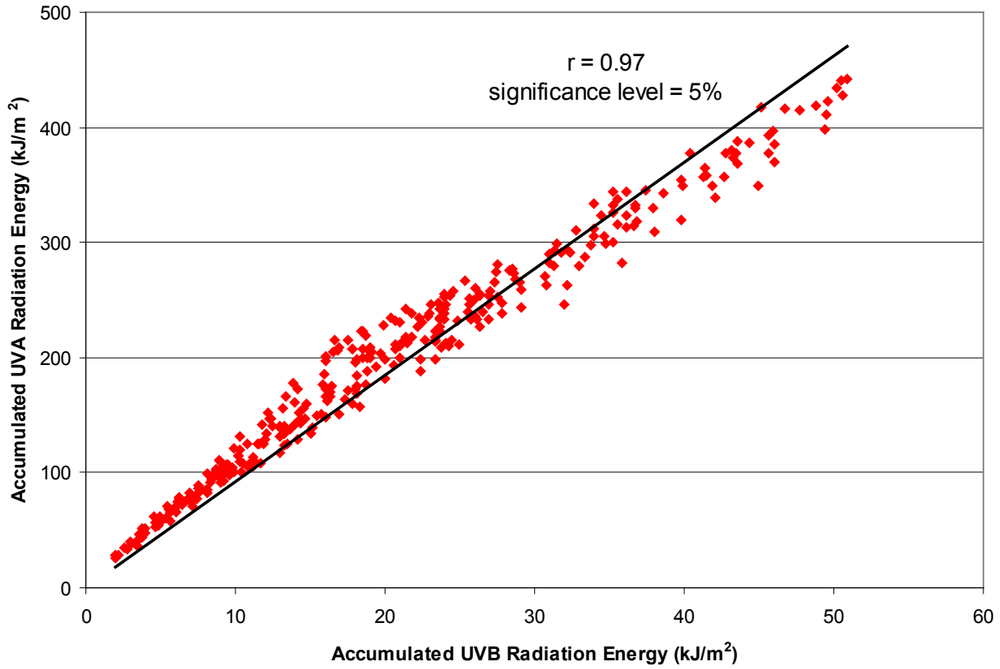

Figure 4. Scatter diagram of daily accumulated UVA and UVB radiation energy (Data period: 1 August 2009 to 31 July 2010)

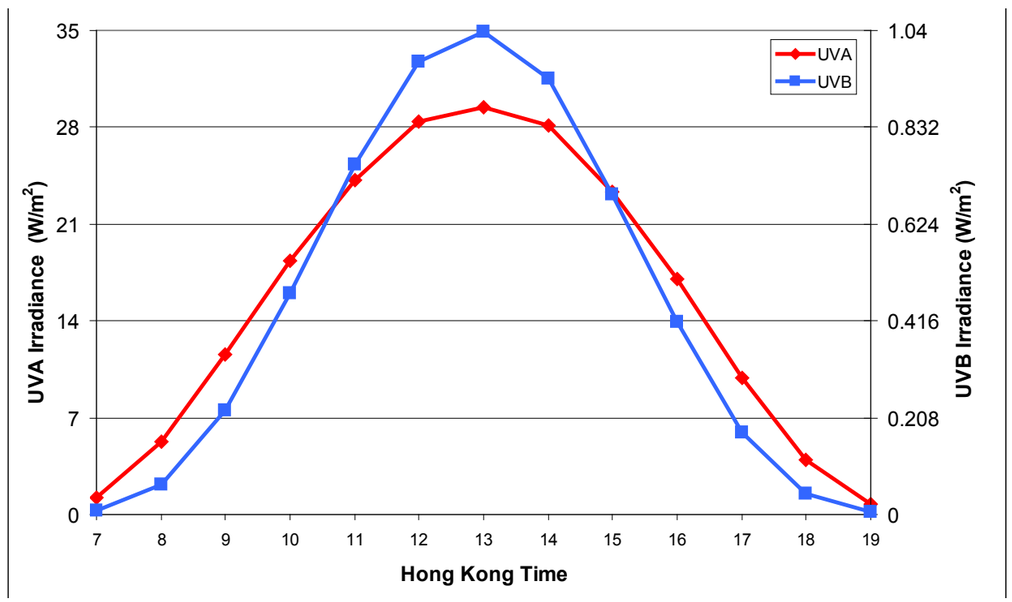

Figure 5. Diurnal variation of hourly UVA and UVB irradiance (Data period: 1 August 2009 to 31 July 2010)

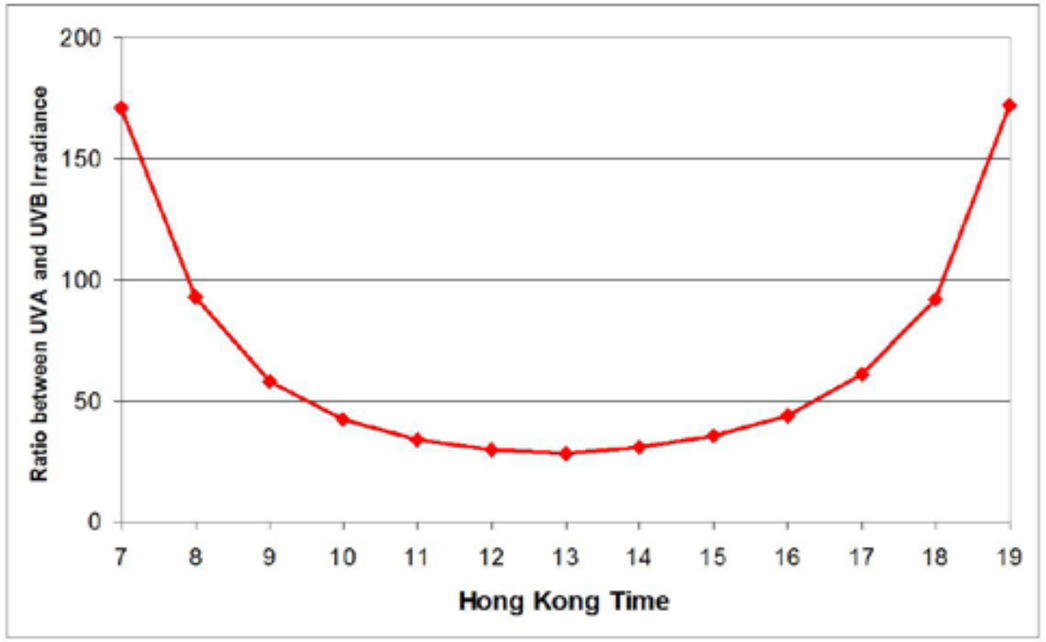

Figure 6. Diurnal variation of the ratio between hourly UVA and UVB irradiance under clear sky condition (total cloud amount 0 to 2 oktas) (Data period: August 2009 to 31 July 2010)

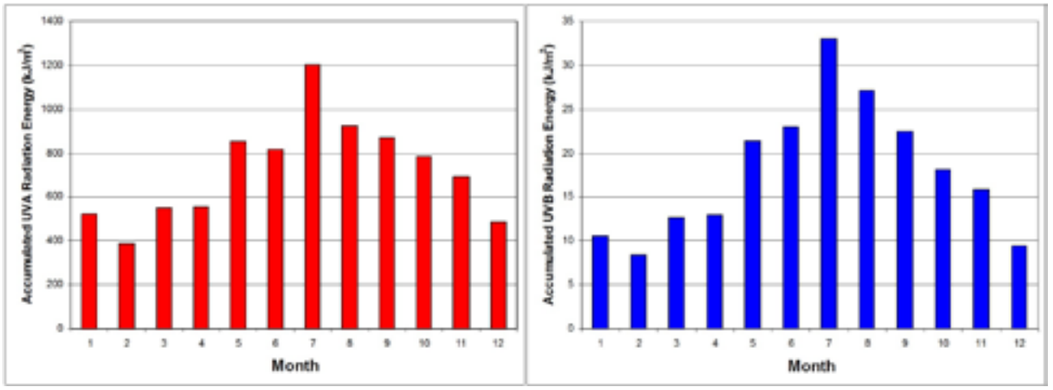

Figure 7. Monthly average of daily accumulated UVA and UVB radiation energy (Data period: 1 August 2009 to 31 July 2010)

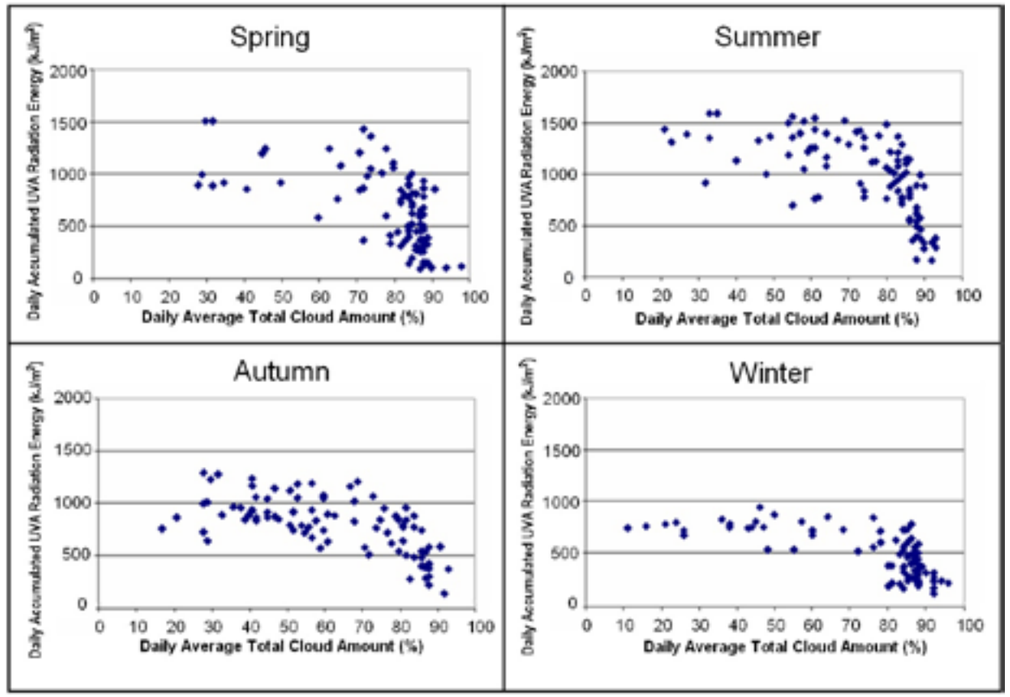

Figure 8. Plots of daily accumulated UVA radiation energy against daily average total cloud amount in different seasons (Data period: 1 August 2009 to 31 July 2010)

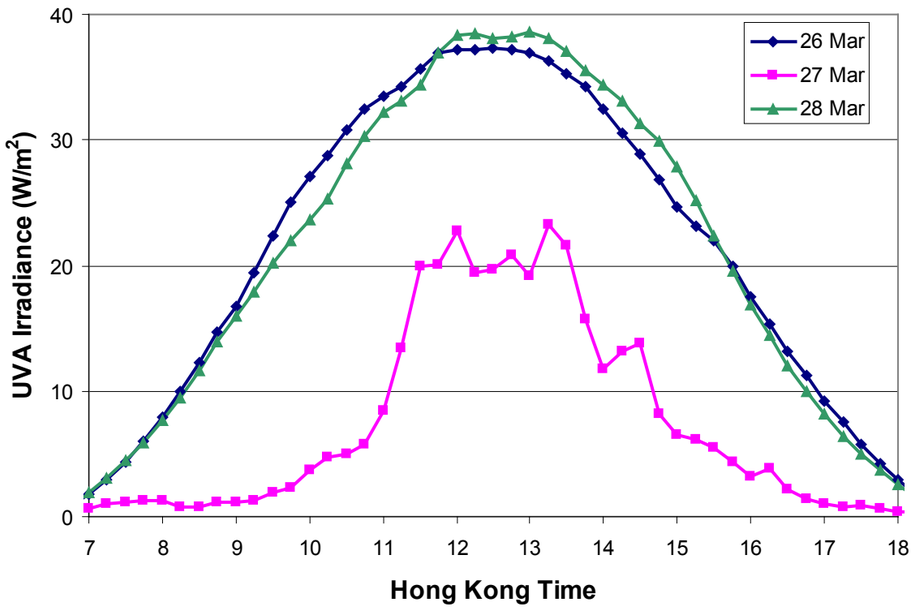

Figure 9. Diurnal variation of UVA irradiance from 26 to 28 March 2010

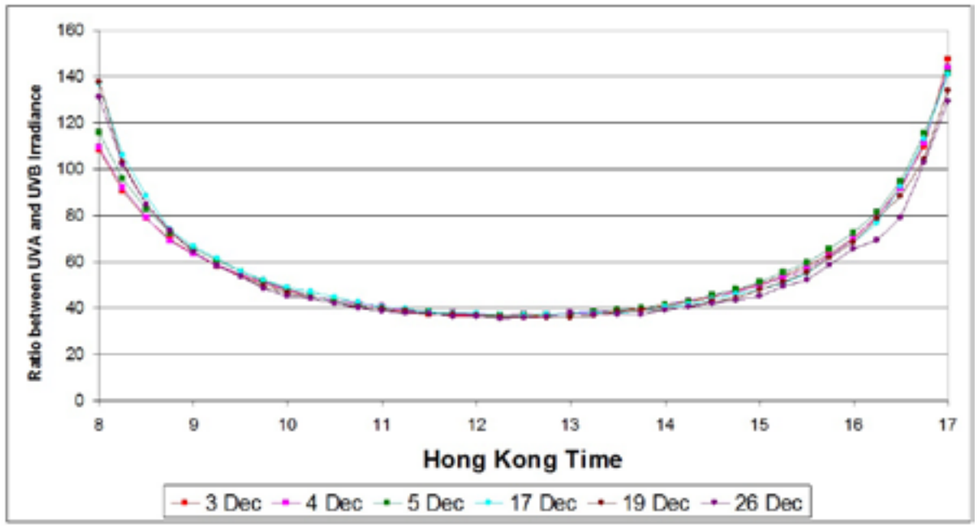

Figure 10. Diurnal variation of the ratio between UVA and UVB irradiance during sunny and cloudy days (sunny days: 3, 4 and 5 December 2010;cloudy days: 17, 19 and 26 December 2010)

Society Event

5 November, 2011
Hong Kong Science Museum
"Wind, Fire, Water and Electricity - Our Living Environment" Lecture Series at the Hong Kong Science Museum

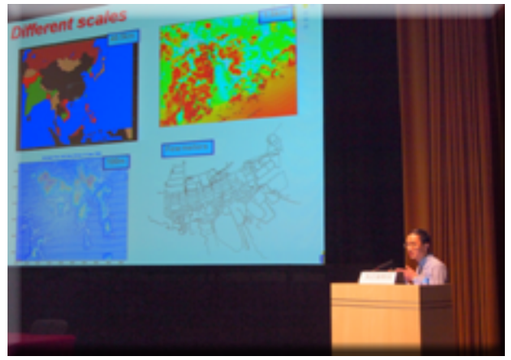

Society Event

International Forum of Meteorological Societies Second Global Meeting (IFMS GM2)

The Second Global Meeting of International Forum of Meteorological Societies (IFMS) was held on 3-4 November 2011. The Chinese Meteorological Society hosted the meeting in Xiamen, China. Participating members include American Meteorological Society, European Meteorological Society, Indian Meteorological Society, East African Meteorological Society, Ethiopian Meteorological Society, Kenya Meteorological Society, Tanzania Meteorological Society, Philippine Meteorological Society, Argentina Meteorological Society, Korean Meteorological Society, Hungarian Meteorological Society, Canadian Meteorological and Oceanographic Society, Australian Meteorological and Oceanographic Society and Hong Kong Meteorological Society.

IFMS is a platform that allows different meteorological societies to get together to discuss management problems and the way forward. In the second meeting, follow up actions raised in first meeting were reported. These include maintenance of the IFMS website, electronic sharing of meteorological societies' bulletins, recruitment of IFMS new members, support of meteorological societies in developing countries, membership benefits, sharing of lectures, experience sharing, coordination with World Meteorological Organization, regional conferences, a unified online newsletter, and financial resources. Other discussion items in the meeting agenda include: (1) Education and Training, (2) Organizing, coordinating and promoting academic exchange activities, (3) Society journals - problems and challenges.

The meeting ended with a plenary wrap-up session. The next meeting was proposed to be held in Europe during the Annual Meeting of the European Meteorological Society in September 2013.

[photos]